Article

Current Biology

A REM-active basal ganglia circuit that regulates anxiety

Graphical abstract

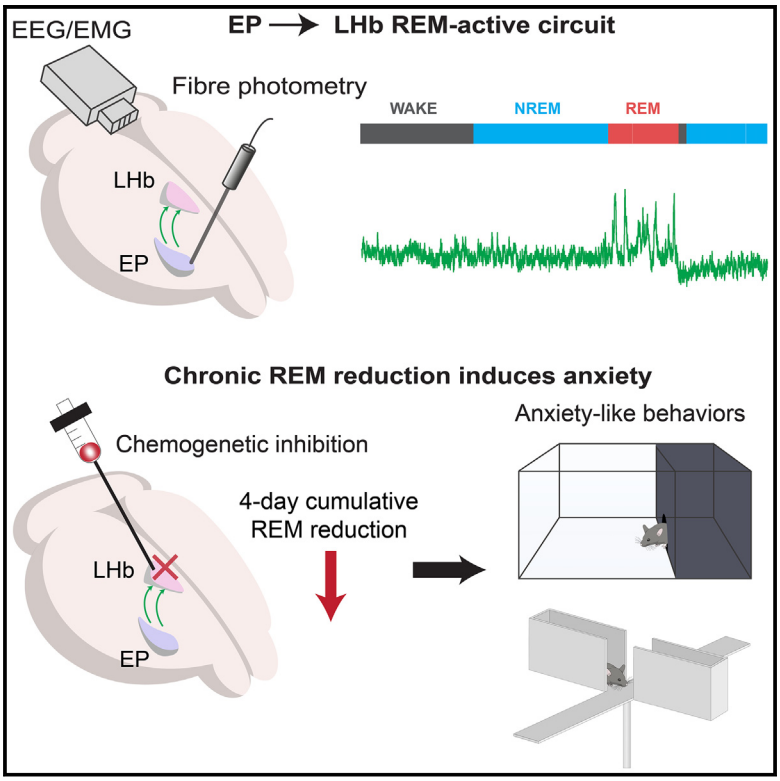

Highlights

- Neurons in the entopeduncular nucleus/internal globus pallidus are REM active
- EP^{Som} neurons regulate REM sleep via the lateral habenula and ventral tegmental area
- Reduction in REM sleep through the EP → LHb → VTA circuit increases anxiety

Authors

Wei Ba, Mathieu Nollet, Chunyu Yin, ..., Alexei L. Vyssotski, William Wisden, Nicholas P. Franks

Correspondence

w.wisden@imperial.ac.uk (W.W.), n.franks@imperial.ac.uk (N.P.F.)

In brief

Ba et al. identify a novel REM sleep-regulating role of the entopeduncular nucleus (EP) → lateral habenula (LHb) circuit. Accumulated reduction in REM sleep due to 4-day suppression of this circuit leads to increased anxiety levels and sensitivity to aversive stimuli.

Ba et al., 2024, Current Biology *34*, 1–14
August 5, 2024
https://doi.org/10.1016/j.cub.2024.06.010

CellPress

Current Biology

CellPress
OPEN ACCESS

Article

A REM-active basal ganglia circuit that regulates anxiety

Wei Ba,[1] Mathieu Nollet,[1,2,5] Chunyu Yin,[1,4,5] Xiao Yu,[1,6] Sara Wong,[1,2] Andawei Miao,[1,2] Esteban J. Beckwith,[1,7] Edward C. Harding,[1,8] Ying Ma,[1,9] Raquel Yustos,[1] Alexei L. Vyssotski,[3] William Wisden,[1,2,*] and Nicholas P. Franks[1,2,10,*]

[1]Department of Life Sciences, Imperial College London, London SW7 2AZ, UK
[2]UK Dementia Research Institute, Imperial College London, London SW7 2AZ, UK
[3]Institute of Neuroinformatics, University of Zurich and ETH Zurich, Zurich 8057, Switzerland
[4]Department of Neonatal Medical Center, Children's Hospital of Nanjing Medical University, Nanjing 210000, China
[5]These authors contributed equally
[6]Present address: Center for Excellence in Brain Science and Intelligence Technology, Chinese Academy of Sciences, Shanghai 200031, China
[7]Present address: Instituto de Fisiología, Biología Molecular y Neurociencias (IFIBYNE), UBA-CONICET, Buenos Aires 1428, Argentina
[8]Present address: Wellcome-MRC Institute of Metabolic Science and MRC Metabolic Diseases Unit, University of Cambridge, Cambridge CB2 0QQ, UK
[9]Present address: State Key Laboratory of Bioelectronics, Zhongda Hospital, School of Life Sciences and Technology, Advanced Institute for Life and Health, Jiangsu Province High-Tech Key Laboratory for Bio-Medical Research, Southeast University, Nanjing 210096, China
[10]Lead contact
*Correspondence: w.wisden@imperial.ac.uk (W.W.), n.franks@imperial.ac.uk (N.P.F.)
https://doi.org/10.1016/j.cub.2024.06.010

SUMMARY

Rapid eye movement (REM) sleep has been hypothesized to promote emotional resilience, but any neuronal circuits mediating this have not been identified. We find that in mice, somatostatin (Som) neurons in the entopeduncular nucleus (EP^{Som})/internal globus pallidus are predominantly active during REM sleep. This unique REM activity is both necessary and sufficient for maintaining normal REM sleep. Inhibiting or exciting EP^{Som} neurons reduced or increased REM sleep duration, respectively. Activation of the sole downstream target of EP^{Som} neurons, Vglut2 cells in the lateral habenula (LHb), increased sleep via the ventral tegmental area (VTA). A simple chemogenetic scheme to periodically inhibit the LHb over 4 days selectively removed a significant amount of cumulative REM sleep. Chronic, but not acute, REM reduction correlated with mice becoming anxious and more sensitive to aversive stimuli. Therefore, we suggest that cumulative REM sleep, in part generated by the EP → LHb → VTA circuit identified here, could contribute to stabilizing reactions to habitual aversive stimuli.

INTRODUCTION

The hypothesis that sleep serves a restorative function has focused largely on non-rapid eye movement (NREM) sleep, the stage of sleep that occurs first.[1] Recently, however, REM sleep in humans has been found to be the deepest and most subjectively satisfying stage of sleep[2,3] and is also the sleep state where capillary blood flow in the mouse brain is selectively boosted.[4] REM sleep has been hypothesized to promote emotional health or resilience,[5–13] for example, in mice, by enabling contextual memory and/or forgetting about emotionally salient stimuli,[14–16] and diverse low-level chronic stressors substantially increase the amount of REM sleep.[5,17] In these situations, more REM sleep could be an adaptation to deal with stress. Similarly, people living with severe depression or post-traumatic stress disorder have elevated REM sleep,[18] a potentially restorative mechanism.[7] An alternative interpretation is that more REM sleep in these conditions could be an abnormality contributing further to pathology.[19] Indeed, monoamine reuptake blockers, taken for depression, markedly decrease REM.[20] These apparent discrepancies as to whether changes in REM sleep are beneficial or harmful remain unresolved.

Although the brainstem circuitry generating atonia during REM is well understood,[21] knowledge of how REM is generated in the forebrain circuitry is incomplete.[22–24] Previously, we found that genetically blocking glutamate release from mouse lateral habenula (LHb) cells produces severe sleep-wake fragmentation,[25] potentially revealing a new sleep-wake pathway. Here, starting by looking at upstream and downstream partners of LHb cells, we found cells in the basal ganglia (the entopeduncular nucleus [EP], also known as the habenula-projecting globus pallidus or GPh, or the internal globus pallidum in primates) projecting to the LHb and then to the ventral tegmental area (VTA) that induce NREM and REM sleep, mapping onto previous circuitry that gets activated with aversion, disappointment, learned helplessness, and anxiety.[26–29] Because of this overlap, we suggest that REM sleep contributes to emotional stability and test this hypothesis by selectively reducing REM sleep originating from this circuit.

Please cite this article in press as: Ba et al., A REM-active basal ganglia circuit that regulates anxiety, Current Biology (2024), https://doi.org/10.1016/j.cub.2024.06.010

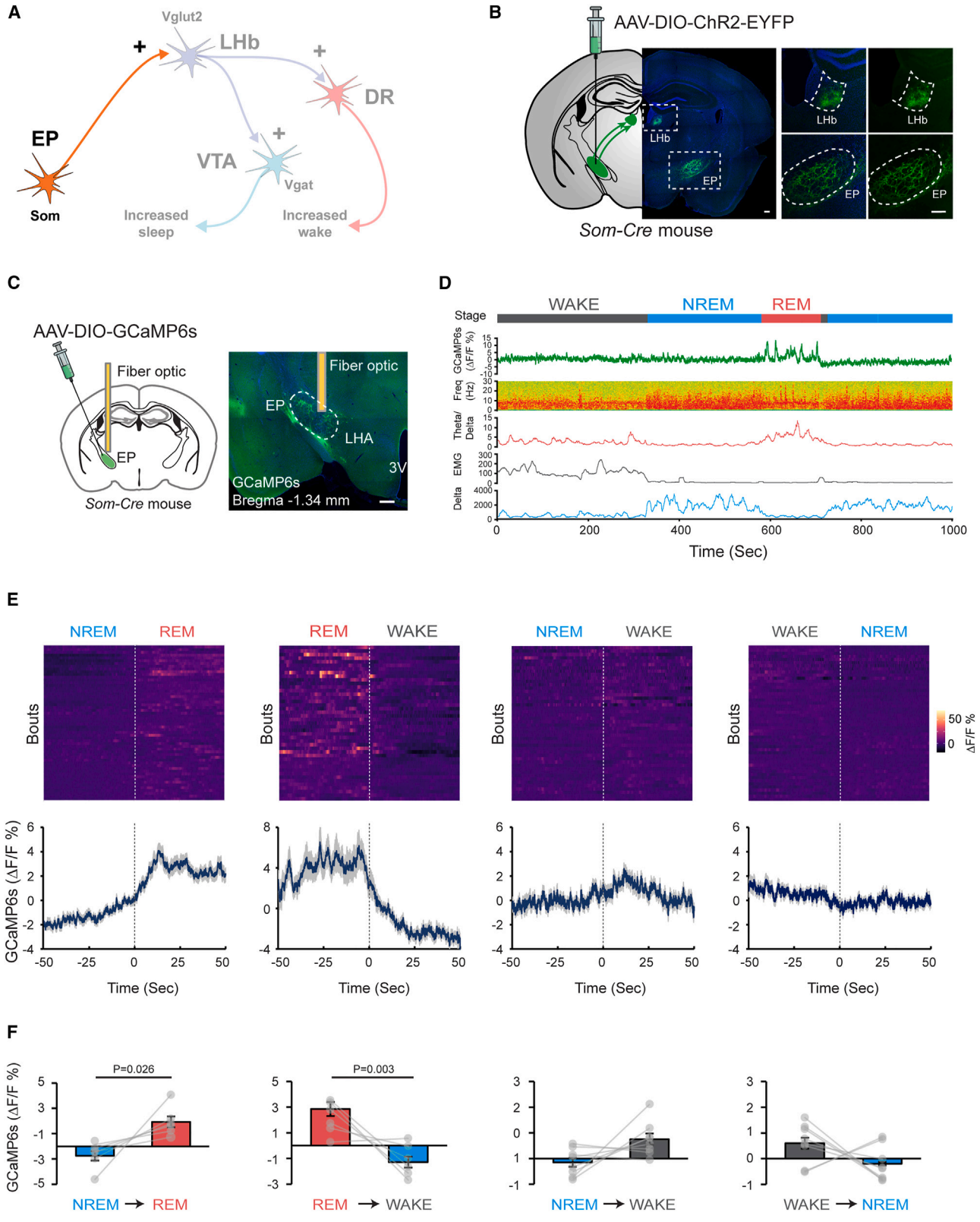

Figure 1. Spontaneous activity of EP^{Som} neurons across sleep-wake states

(A) Conceptual schematic diagram of the neuronal circuit examined in this figure. EP, entopeduncular nucleus; LHb, lateral habenula; DRN, dorsal raphe nucleus; VTA, ventral tegmental area.

(legend continued on next page)

Please cite this article in press as: Ba et al., A REM-active basal ganglia circuit that regulates anxiety, Current Biology (2024), https://doi.org/10.1016/j.cub.2024.06.010

RESULTS

EP^{Som} neurons are strongly REM sleep active

The LHb receives diverse inputs[30–35] but including a unique projection from somatostatin (Som)-glutamate-GABA neurons in the EP.[26,36–38] We performed anterograde tracing by injecting *AAV-DIO-ChR2-EYFP* in the EP of *Som-Cre* mice and confirmed that EP^{Som} neurons project exclusively to the LHb as previously reported[26,36,39–41] (Figures 1A and 1B). We then used calcium photometry to study the natural dynamics of the EP^{Som} neurons across the sleep-wake cycle. *AAV-DIO-GCaMP6s* was injected into the EP of *Som-Cre* mice, with an optical fiber implanted over the EP to acquire population activity of EP^{Som} neurons (Figures 1C and S1A). We observed the highest activity of EP^{Som} neurons during REM sleep, while the activity during NREM sleep and wakefulness was suppressed (Figures 1D–1F). The baseline Ca^{2+} transients began to elevate at the end of NREM episodes, and we observed a time-locked increase (p = 0.026; n = 6) at the transition from NREM to REM. Conversely, the fluorescence signal decreased (p = 0.003; n = 8) during REM-WAKE transitions. Recordings from EP^{Som}-GFP control mice displayed no such vigilance state-dependent variations (Figures S1B and S1C).

EP^{Som} neurons bidirectionally regulate REM sleep

To assess whether EP^{Som} activity is necessary for natural REM sleep, we inhibited these neurons chemogenetically. *AAV-DIO-hM4Di-mCherry* (referred to as "hM4Di" hereafter) was bilaterally injected into the EP of *Som-Cre* mice (Figures 2A and S2A). The inhibitory effect of the hM4Di receptors was confirmed by the strongly reduced number of c-Fos-expressing cells in the EP following clozapine-*N*-oxide (CNO) administration (Figure S2B; p = 0.002; n = 3). Our preliminary tests indicated a sleep-suppressing trend when inhibiting EP^{Som} neurons. We further evaluated this effect during the lights-on phase when mice are mostly inactive and show abundant sleep. Systemic administration of 1 mg/kg CNO at the beginning of the lights-on phase significantly (p = 0.0004; n = 7) reduced the total duration of REM sleep during the 3 h following CNO injection, as compared with saline-injected controls (Figures 2B–2D). Reduced REM sleep amounts were due to decreased numbers of long (>1 min) REM-sleep episodes (from 54% to 29%; p = 0.03; n = 7). Short REM-sleep episodes (<1 min) remained unaffected. By contrast, total duration of wakefulness and NREM sleep remained unchanged (Figures 2B–2D). Furthermore, chemogenetic inhibition of EP^{Som} neurons significantly (p = 0.02; n = 7) increased the latency to REM sleep without affecting NREM latency (Figure 2D).

We next selectively lesioned EP^{Som} cells using *AAV-DIO-CASP3* injected into the EP of *Som-Cre* mice (Figure S2C). In the control *AAV-DIO-mCherry* group, 91.2% of mCherry-expressing neurons were co-labeled with anti-SOM antibodies (Figure S2D), and the posterior EP was found to contain a high density of SOM neurons (Figure S2E). After selective expression of caspase in EP^{Som} cells, immunohistochemistry staining for SOM revealed that 89% of SOM cells were eliminated (Figures S2F and S2G; p = 0.009; n = 4). 4 weeks after the lesions, shortened times in REM sleep were also observed (Figures 2E and 2F). Following ablation, the total duration of REM sleep in the light phase consistently (p = 0.0004; n = 8 control and n = 11 caspase) declined, further confirming that these neurons contribute to normal REM sleep structure. This effect was selectively confined to the 12-h light part of the daily cycle.

To examine whether EP^{Som} neurons can elicit REM sleep in fully awake mice, we expressed *AAV-DIO-hM3Dq-mCherry* (referred to as "hM3Dq" hereafter) in the EP^{Som} neurons (Figures 2G and S3A) and performed intraperitoneal (i.p.) injections of saline or CNO in the dark period when mice show high levels of arousal. Compared with the saline control group, 1 mg/kg CNO injection increased the number of c-Fos positive neurons in the EP (Figure S3B; p = 0.001; n = 3) and induced NREM and REM sleep (Figure 2H). The total duration of both NREM and REM sleep significantly (p = 0.03 and p = 0.04, respectively; n = 7) increased during the 6 h post CNO injection (Figures 2I and 2J). The latencies to both NREM and REM sleep were reduced (p = 0.0008 and p = 0.008, respectively; n = 7) by CNO (Figure 2J). Given that EP^{Som} neurons are silent during NREM sleep and that REM sleep only occurs following NREM sleep in physiological conditions, we interpret the increased NREM sleep as a necessary element for inducing REM sleep.

To achieve higher temporal precision, we conducted optogenetic activation experiments and assessed sleep structure after brief excitation of the EP^{Som} neurons. *AAV-DIO-ChR2-EYFP* or *AAV-DIO-GFP* was expressed in the EP^{Som} neurons (Figure S4A), and sleep-wake states were monitored and compared between "laser on" and "laser off" conditions. Stimulation with light was confirmed as excitatory, as it increased c-FOS expression in the EP (Figures S4B and S4C). When laser stimulation was delivered during NREM sleep, the percentage of REM sleep increased (Figure S4D; p = 0.003, n = 4). On the contrary, brief optogenetic stimulation of the EP^{Som} neurons during WAKE did not alter the amount of sleep or WAKE. Together, these data support a role for EP^{Som} neurons in REM sleep regulation.

(B) Anterograde tracing confirms that EP^{Som} neurons project exclusively to the LHb. Representative images of the cell bodies in the EP and terminals in the LHb after *AAV-DIO-ChR2-EYFP* was injected into the EP of *Som-Cre* mice. Left: a coronal section includes both EP and LHb (indicated in dashed boxes). Anatomical scheme adapted from Paxinos and Franklin.[42] Right: ChR2-EYFP-expressing neurons in the EP and its projections in the LHb with higher magnification. No projections in other brain areas were observed. Blue, nuclei stained with Hoechst 33342; green, ChR2-EYFP. Scale bars, 100 μm.
(C) Fiber photometry with EEG/EMG recordings in freely moving mice. *AAV-DIO-GCaMP6s* was injected into the EP of *Som-Cre* mice, and a fiber optic was implanted above the EP to record activity (scale bar, 200 μm). LHA, lateral hypothalamic area; 3V, third ventricle.
(D) Representative fiber-photometry recording aligned with the EEG spectra and EMG recordings during wakefulness, NREM, and REM sleep.
(E) Combined fluorescence responses during transitions between vigilance states for all mice (n = 6–8). Top: individual traces with color-coded fluorescence intensity. Bottom: mean responses of each transition (blue) ± SEM (gray).
(F) Summary of transitions between states. p values are given when <0.05.
See also Figure S1.

Please cite this article in press as: Ba et al., A REM-active basal ganglia circuit that regulates anxiety, Current Biology (2024), https://doi.org/10.1016/j.cub.2024.06.010

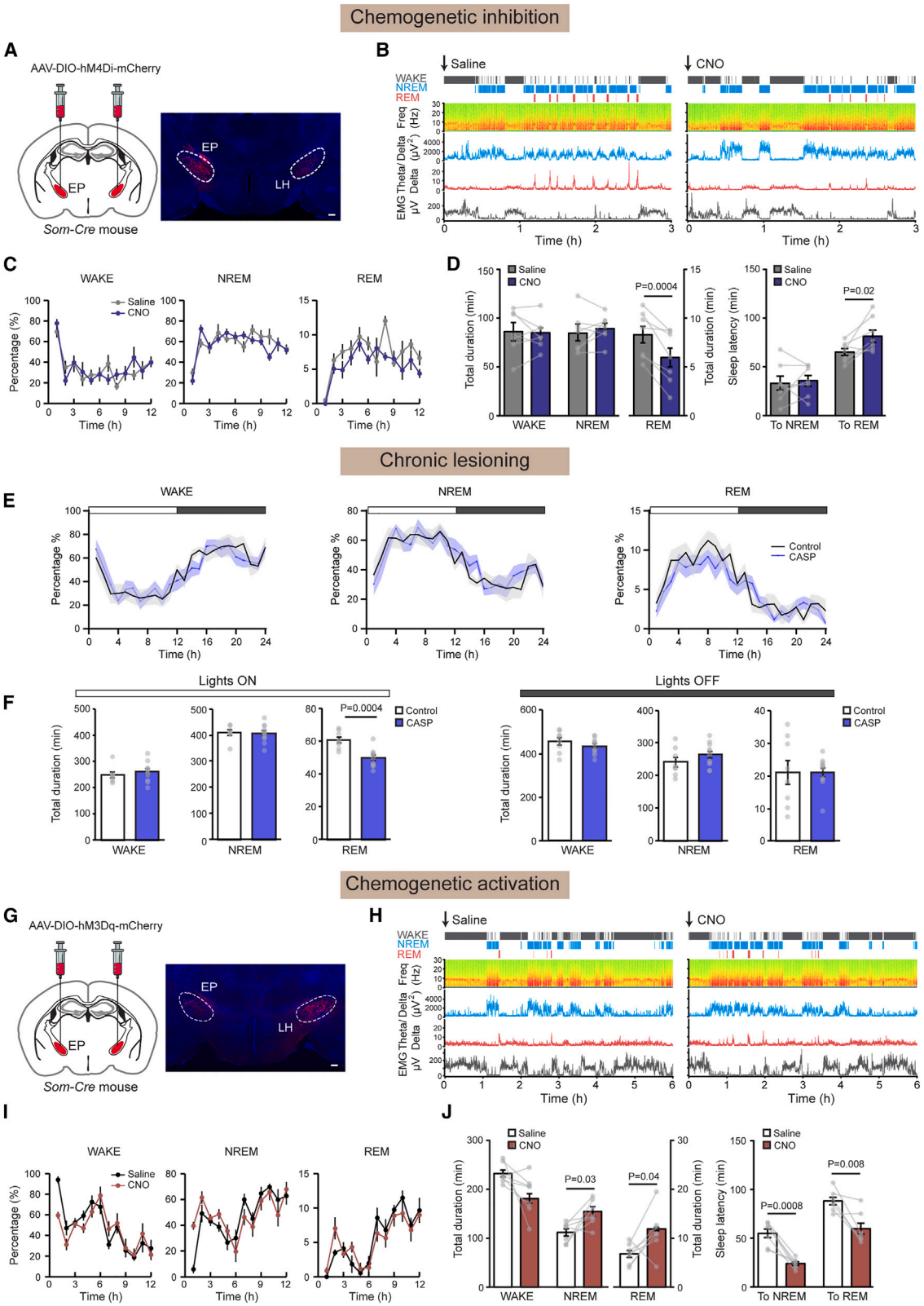

(legend on next page)

EP^{Som} neurons regulate REM sleep via their sole target, the LHb

We reasoned that EP^{Som} neurons regulate REM sleep via their sole downstream target, the LHb. We first validated the excitatory nature of the projections from EP^{Som} neurons onto the LHb. Chemogenetically exciting the EP^{Som} neurons with hM3Dq receptors and i.p.-injected CNO increased the number of c-Fos-expressing neurons in the LHb (Figure S5A; $p = 0.018$; $n = 3$). Three experiments were then carried out to confirm our hypothesis. First, we examined whether the output from EP to LHb correlated with REM sleep by monitoring the Ca^{2+} transients at EP → LHb terminals. We injected *AAV-DIO-GCaMP6s* in EP^{Som} neurons and positioned the optical fiber over the LHb. Our results showed that as for the EP^{Som} somata, the Ca^{2+} transients at EP → LHb terminals were the highest during REM sleep (Figure S5B). NREM-REM sleep transitions were associated with prominent increases of activity at these terminals (Figure S5C; $p = 0.0002$; n = 5). Next, we examined whether the LHb is similarly modulated during REM sleep by measuring the Ca^{2+} transients in the cell bodies of LHb neurons across the sleep-wake cycle (Figures 3A and 3B) (note: we used *Vglut2* gene expression as a local selective marker for LHb cells so as not to get contaminating expression from the overlying hippocampal dentate granule cells). We found that LHb^{Vglut2} neurons were most active during wakefulness and REM sleep and suppressed during NREM sleep (Figures 3C–3E). The Ca^{2+}-induced fluorescence increased significantly at NREM to REM transitions. Conversely, LHb^{Vglut2} activity decreased when animals entered NREM sleep. Interestingly, the activity in the LHb during wakefulness is attributed, at least in part, to its excitatory input from the lateral preoptic area (LPO) (Figure S6). Finally, we examined whether the LHb^{Vglut2} neurons can bidirectionally regulate REM sleep. We expressed hM4Di in LHb^{Vglut2} neurons and performed electroencephalogram (EEG)/electromyogram (EMG) analysis comparing control saline injections with CNO injections (Figure 4A). CNO-mediated inhibition of LHb^{Vglut2} neurons reduced the number of c-FOS-expressing cells (Figures S7A and S7B) and decreased REM sleep duration, leaving NREM sleep and wakefulness intact (Figures 4B–4D). This reduction was due to fewer REM episodes (Figure S7C). Conversely, chemogenetically activating LHb^{Vglut2} neurons prolonged both NREM and REM sleep at the expense of wakefulness (Figures 4E–4H). Increased episode number and duration of REM sleep were observed (Figure S7D). In control experiments, CNO (1 mg/kg; i.p.) had no effect on vigilance states in *Vglut2-Cre* mice (Figure S8). Taken together, these findings reveal a close correlation of LHb activity with REM sleep as well as a capacity of the LHb for the bidirectional regulation of REM sleep, thereby supporting the idea that the EP → LHb circuit contributes to maintaining normal REM sleep.

LHb → VTA terminals are most active during REM sleep, and their selective activation promotes REM sleep

We next sought to identify the output pathway from the LHb mediating the REM-sleep-regulating effect. Previous studies identified multiple synaptic targets of the glutamatergic LHb neurons. We focused on the dorsal raphe nucleus (DRN) and the VTA,[30] two areas modulating motivation/aversion and previously identified as contributing to sleep-wake regulation.[43,44] We first validated LHb → DRN and LHb → VTA connectivity using c-FOS mapping and found that activating LHb^{Vglut2} neurons increased the number of c-FOS-expressing neurons in the DRN and the VTA (Figures S9A–S9F). 10.7% of the activated VTA neurons are dopaminergic (Figures S9G and S9H). *In vivo* fiber-photometry recordings at LHb → DRN and LHb → VTA terminals across sleep-wake cycles were achieved similarly as described above, by expressing *AAV-DIO-GCaMP6s* in LHb^{Vglut2} neurons, and with optical fibers placed over terminals in either the DRN or VTA (Figures 5A and 5C). We observed a wake-specific calcium signal at the LHb → DRN terminals, while the activity was absent during sleep (Figures 5B and S10); indeed, the LHb → DRN projection has been found to induce aggressive arousal.[45] By contrast, NREM-REM transitions were consistently associated with prominent increases in the activity of LHb → VTA terminals (Figures 5C–5E). To further establish whether the LHb promotes sleep through its projections to the VTA, we expressed hM3Dq in the LHb and unilaterally delivered CNO, via a cannula, into the VTA to excite the LHb glutamatergic terminals (Figure S11A). Infusing CNO (0.2 μL of 3 μM, over 5 min) into the VTA elicited both NREM and REM sleep, recapitulating the effects of activating the LHb somata (Figures S11B and S11C).

Chronic REM sleep restriction increases anxiety levels and alters defensive behavior

We assessed the functional significance of REM sleep generated by the circuit. We initiated our tests by targeting the LHb due to its

Figure 2. EP^{Som} neurons are sufficient and necessary for normal REM sleep

(A–D) Chemogenetic inhibition of EP^{Som} neurons suppresses REM sleep.

(A) Schematic illustrating inhibition of EP^{Som} neurons using DREADD receptors. *AAV-DIO-hM4Di-mCherry* was injected into the EP of *Som-Cre* mice. Immunostaining confirmed the expression of hM4Di-mCherry in the EP. LH, lateral hypothalamus; scale bar, 200 μm.

(B) Representative EEG/EMG recordings post-saline or CNO (1 mg/kg) injections.

(C) 12 h sleep recording post-saline (gray) or CNO (purple) injection. Data are mean ± SEMs.

(D) Summarized changes on sleep duration and latency. Data are mean ± SEMs ($n = 7$). p values are given when <0.05.

(E and F) Sleep analysis of control and CASP3 mice.

(E) 24 h sleep recording post-saline (black) or CNO (blue) injection. Data are mean ± SEMs.

(F) Quantification of each vigilance state in the lights-on or lights-off phases. Lesioning of EP^{Som} neurons reduced REM sleep duration in the lights-on phase without affecting NREM and wakefulness ($p = 0.0004$, control $n = 8$, CASP $n = 11$). Data are mean ± SEMs. p values are given when <0.05.

(G–J) Chemogenetic activation of EP^{Som} neurons increases sleep.

(G) Schematic of activation of EP^{Som} neurons using DREADD receptors. *AAV-DIO-hM3Dq-mCherry* was injected into the EP. LH, lateral hypothalamus; scale bar, 200 μm.

(H) Representative traces of EEG/EMG recordings post-saline or CNO injections.

(I) 12 h sleep recording post-saline (black) or CNO (red) injection. Data are mean ± SEMs.

(J) Summarized changes of sleep duration and latency. Data are mean ± SEMs ($n = 7$). p values are given when <0.05.

See also Figures S2–S4.

Please cite this article in press as: Ba et al., A REM-active basal ganglia circuit that regulates anxiety, Current Biology (2024), https://doi.org/10.1016/j.cub.2024.06.010

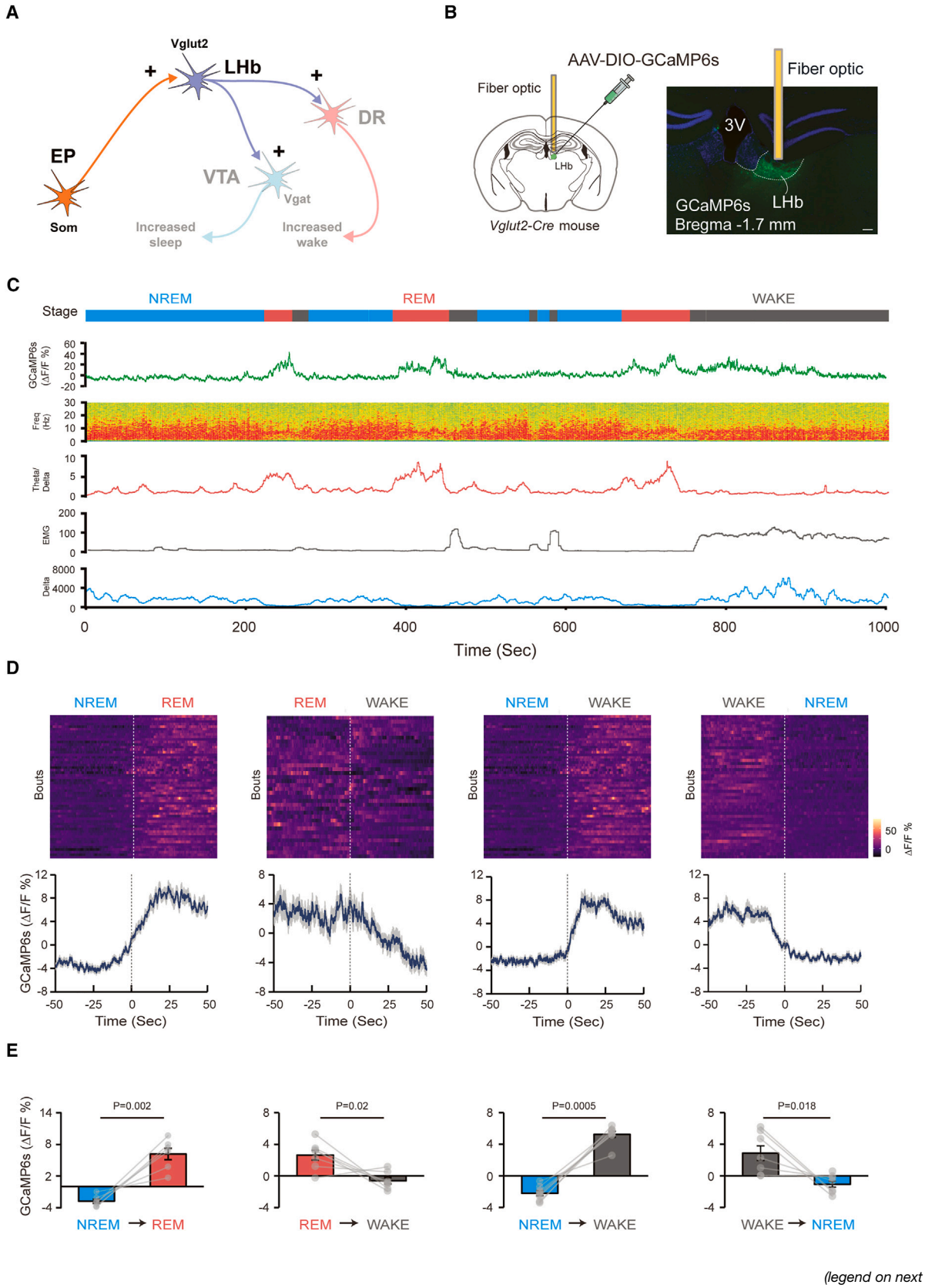

(legend on next page)

Please cite this article in press as: Ba et al., A REM-active basal ganglia circuit that regulates anxiety, Current Biology (2024), https://doi.org/10.1016/j.cub.2024.06.010

more pronounced impact on REM sleep and discovered that repetitive dosing of LHb$^{Vglut2\text{-}hM4Di}$ mice with CNO led to a chronic reduction of REM sleep. LHb$^{Vglut2\text{-}hM4Di}$ mice were given saline or CNO once a day at the beginning of the inactive lights-on phase for 4 consecutive days. This reduced REM sleep by 24%, 15%, 11%, and 7% over the 4 days but did not change the measurable amount of NREM sleep or wake (Figure S12). Then, 16 h after the last saline or CNO administration on day 4, mice were evaluated in several behavioral tests (Figure 6A). In the light-dark test (Figure 6B), mice with reduced REM sleep increased their time in the dark compartment with a corresponding decrease in the light chamber. General locomotion of the LHb$^{Vglut2\text{-}hM4Di}$ mice injected with saline or CNO remained unchanged, as indicated by the same amount of entry numbers into the chambers (Figure 6B). Similarly, compared with control mice, LHb$^{Vglut2\text{-}hM4Di}$ mice spent less time in the open arm in an elevated plus maze test when REM sleep was suppressed (Figure 6C). To examine how the EP^{Som} neurons contribute to anxiety behaviors, the same paradigm of a 4-day chemogenetic inhibition was used in EP$^{Som\text{-}hM4Di}$ mice, followed by assessing their level of anxiety. There was a less pronounced REM sleep-suppressing effect within EP$^{Som\text{-}hM4Di}$ mice compared with that observed in the LHb$^{Vglut2\text{-}hM4Di}$ mice, as REM was only significantly suppressed on the first day (Figure S13). Nevertheless, in the light-dark test, EP$^{Som\text{-}hM4Di}$ mice injected with CNO for 4 days spent more time in the dark compartment (Figures S14A–S14C). On the other hand, acute opto-exciting the EP^{Som} neurons (EP$^{Som\text{-}ChR2}$ mice) did not produce any behavioral changes (Figure S14D).

To further assess whether REM sleep contributes to the performance of innate behaviors, such as defensive behaviors, we performed a looming test in which a moving disk is presented to mimic distal threats. In this test, mice generally respond with freezing behaviors.[46] When REM sleep was restricted for 4 days by inhibiting LHb cells, CNO-treated LHb$^{Vglut2\text{-}hM4Di}$ mice responded to the stimuli much faster than the control group, indicated by reduced latencies to freeze (Figure 6D). The duration of freezing behaviors was unaltered, however (Figure 6D). Thus, REM sleep deficits induced sensitization of defensive responses to visual threats. We observed no change in the marble burying test (Figure 6E), indicating that reducing REM sleep did not induce repetitive behaviors in mice. Overall, the behavioral results show that cumulative baseline REM sleep could contribute to stabilizing behavioral reactions to habitual aversive stimuli and reducing anxiety-like behaviors.

DISCUSSION

The pathways that contribute to REM sleep generation are still being elucidated.[21–24,47–50] The basal ganglia, a collection of subcortical nuclei that include the nucleus accumbens, the caudate-putamen, the GPh externa, the EP (GPh interna), and the substantia nigra, have all been implicated in the induction of NREM sleep or wakefulness, depending on the specific cell type.[51–54] By contrast, the strongly REM-active nature of the EP^{Som} cells in basic home cage conditions of the mice is a striking feature of our findings. These EP^{Som} cells are unusual in that in both primates and rodents, they project to just one target, the LHb,[37] a nucleus that we previously showed is needed for consolidated sleep.[25] The same circuitry of EP^{Som} cells and their downstream target, the LHb cells, fires with aversive events or disappointment,[26,28,29] in other words, when an outcome is worse than expected.[30,55] This EP → LHb → VTA circuit helps animals learn about negative experiences and/or adopt passive coping strategies.[55–57] That this circuitry seems to have an exact mapping with the REM sleep circuitry we report here seems more than a coincidence. Empirically, we discovered that a simple scheme to periodically chemogenetically inhibit the LHb over 4 days selectively removed a significant amount of cumulative REM sleep, without affecting measurable amounts of NREM or wakefulness. Testing 16 h later after the last inhibitory dose, chronic REM reduction correlated with mice becoming more sensitive to aversive stimuli. Of note, acute activation of the EP → LHb circuit did not have anxiolytic effects, indicating that the altered anxiety levels may stem from accumulated changes in REM sleep. Therefore, we suggest that baseline cumulative REM sleep could contribute to stabilizing reactions to habitual aversive stimuli.

The LHb is a relay nucleus with many channels (reflecting diverse inputs) and receives innervations from about forty brain regions, including from the EP, but also from the hypothalamus, midbrain, and brainstem areas.[30–33,35] Some of these other inputs to the LHb are also REM active and could contribute to driving the LHb during REM, and this could explain why we see larger effects for the LHb modulating REM sleep on behavior than modulating the EP nucleus alone. There are multiple REM drivers to the LHb. For example, glutamate neurons in the lateral hypothalamus project to the LHb and are both wake and REM sleep active.[58] On the other hand, our data showed that the input from the preoptic area of the hypothalamus is selectively active during wakefulness, likely contributing to the wake-active calcium signals in the LHb we observed together with other WAKE-active upstream inputs.

All subtypes of LHb cells release glutamate onto distal targets, and a few likely co-release GABA and glutamate.[33] We found that the outputs to the dorsal raphe are not sleep-active, but the LHb terminals in the VTA are and could induce sleep by activating GABA neurons, potentially feeding into a circuit we identified for how certain stressors (social defeat stress) induce sleep.[59] In social defeat stress, hypothalamic and brainstem

Figure 3. Spontaneous activities of LHb^{Vglut2} neurons across sleep-wake

(A) Conceptual schematic circuit diagram. EP, entopeduncular nucleus; LHb, lateral habenula; DRN, dorsal raphe nucleus; VTA, ventral tegmental area.

(B) Fiber photometry with EEG/EMG recordings in freely moving mice. Left: schematic illustration of experimental setup. Right: *AAV-DIO-GCaMP6s* was injected into the LHb of *Vglut2-Cre* mice, and a fiber optic was implanted above the LHb to record activity; 3V, third ventricle (scale bar, 100 μm).

(C) Representative Ca^{2+} signals aligned with the EEG spectra and EMG recordings during wakefulness, NREM, and REM sleep.

(D) Combined fluorescence responses during transitions between vigilance states for all mice (n = 6–8). Top: individual traces with color-coded fluorescence intensity. Bottom: mean responses of each transition (blue) ± SEM (gray).

(E) Summary of transitions between states. Data are mean ± SEMs. p values are given when <0.05.

See also Figures S5 and S6.

Please cite this article in press as: Ba et al., A REM-active basal ganglia circuit that regulates anxiety, Current Biology (2024), https://doi.org/10.1016/j.cub.2024.06.010

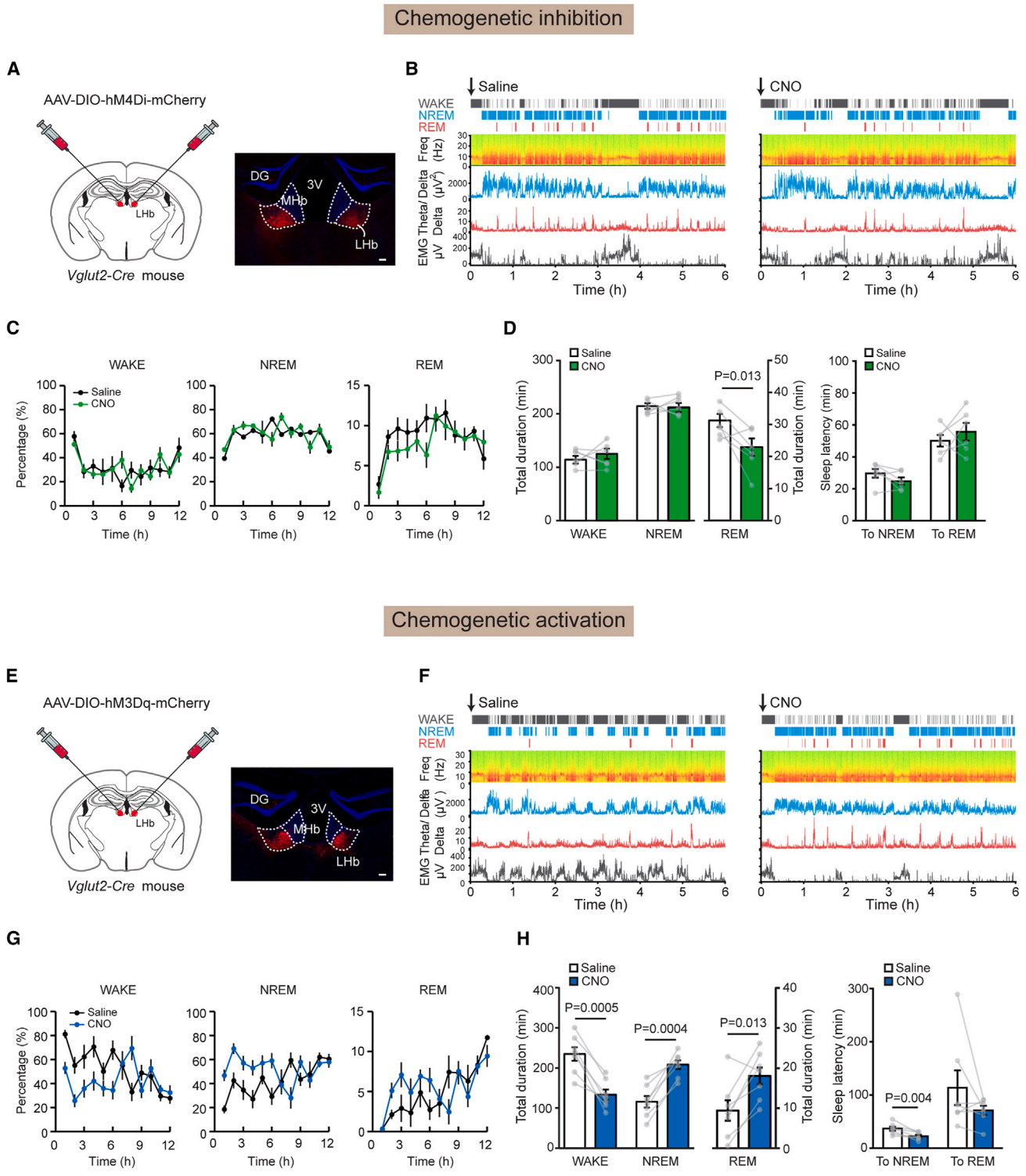

Figure 4. Causal effects of LHb^{Vglut2} neurons on REM sleep

(A–D) Chemogenetic inhibition of LHb^{Vglut2} neurons suppresses REM sleep.

(A) Schematic illustrating inhibition of LHb^{Vglut2} neurons using DREADD receptors. *AAV-DIO-hM4Di-mCherry* was injected into the LHb of *Vglut2-Cre* mice. Immunostaining confirmed the expression of hM4Di-mCherry in the LHb. DG, dentate granule cells; MHb, medial habenula; 3V, third ventricle; scale bar, 100 μm.

(B) Representative EEG/EMG recordings post-saline or CNO (1 mg/kg) injection.

(C) 12 h sleep recording post-saline (black) or CNO (green) injection. Data are mean ± SEMs.

(D) Summarized changes on sleep duration and latency. Data are mean ± SEMs (n = 7). p values are given when <0.05.

(E–H) Effects of chemogenetic activation of LHb^{Vglut2} neurons on sleep.

(legend continued on next page)

stress pathways activate VTA GABA cells to promote sleep.[59] But milder stress and habitual aversive stimuli could activate the VTA sleep circuitry via the EP^{Som} → LHb branch to regulate sleep. A further feature is that EP^{Som} cells co-release both GABA and glutamate, so they can simultaneously excite via ionotropic glutamate receptors and inhibit via $GABA_A$ receptors the post-synaptic LHb cells.[38] Our c-FOS-mapping results indicate that the EP^{Som} cells predominately excite the LHb, in line with previous reports.[36] Based on our results, the glutamate component would be predicted to enhance REM, and the GABA component decrease REM sleep. But given that the balance of glutamate and GABA transmission at EP^{Som} to LHb synapses could vary with different behaviors, motivations, and stressors,[38,60,61] certain stressors and experiences could enhance REM sleep, whereas others could decrease it.

An overlap exists between the consequences of activating the EP → LHb → VTA sleep circuit we have identified and the state of depression. Non-medicated depressed patients often enter REM sleep more quickly, and their REM lasts longer.[18] Moreover, the LHb is more active during depression,[62] and we predict that it is this habenula overactivity that causes the enhanced REM in this condition. The enhanced REM in people living with depression is often assumed to be an adverse outcome. However, this enhanced REM could, in fact, be beneficial and aid emotional processing rather than being harmful. Indeed, this logic suggests that drugs or other treatments that selectively enhance REM might be beneficial in treating depression (current drugs suppress REM sleep[20]). Thus, understanding the sleep-promoting aspects of the EP → LHb → VTA circuitry could allow insights to improve mental health.

STAR★METHODS

Detailed methods are provided in the online version of this paper and include the following:

- KEY RESOURCES TABLE
- RESOURCE AVAILABILITY
  - Lead contact
  - Materials availability
  - Data and code availability
- EXPERIMENTAL MODEL AND STUDY PARTICIPANT DETAILS
- METHOD DETAILS
  - Viral constructs and preparation
  - Stereotaxic surgery
  - EEG and EMG recording and scoring of sleep-wake behaviors
  - Immunohistochemistry
  - Fiber photometry
  - Behavioral Tests
- QUANTIFICATION AND STATISTICAL ANALYSIS

SUPPLEMENTAL INFORMATION

Supplemental information can be found online at https://doi.org/10.1016/j.cub.2024.06.010.

ACKNOWLEDGMENTS

This research supported by the Wellcome Trust (107839/Z/15/Z, 107841/Z/15/Z, and 220759/Z/20/Z, N.P.F. and W.W.); the UK Dementia Research Institute (award number UK DRI-5004) through UK DRI Ltd, principally funded by the Medical Research Council (W.W. and N.P.F.); the Rubicon Research Program of the Netherlands Organization for Scientific Research (NWO) (019.161LW.010, W.B.) and the People Program (Marie Curie Actions) of the European Union's Eight Framework Program H2020 under REA grant agreement 753548 (W.B.); the National Natural Science Foundation of China (grant no 82201700, C.Y.); the Outstanding Youth Project from Nanjing Health and Health Commission (no JQX23009, C.Y.); and a Cross-Centre UK Dementia Research Institute post-doctoral award (S.W.). The Facility for Imaging by Light Microscopy (FILM) at Imperial College London was in part supported by funding from the Wellcome Trust (grant 104931/Z/14/Z) and BBSRC (grant BB/L015129/1). We thank A. Bruckbauer for the technical support with the microscopes; V. Navetat for helping with some of the illustrations; and M. Stephenson-Jones, F. Marbach, and L. Rollik (Sainsbury Wellcome Center, UCL) for valuable discussions. For the purpose of open access, the author has applied a CC BY public copyright license to any Author Accepted Manuscript version arising from this submission.

AUTHOR CONTRIBUTIONS

W.B. conceived the project. N.P.F. and W.W. supervised the work. W.B. designed and performed most experiments and data analysis. M.N., X.Y., and Y.M. performed some behavioral tests. E.J.B. and E.C.H. performed some data analysis. C.Y., S.W., A.M., and R.Y. performed some histology experiments. A.L.V. developed the neurologgers. W.B., W.W., and N.P.F. wrote the manuscript.

DECLARATION OF INTERESTS

The authors declare no competing interests.

Received: June 12, 2023
Revised: April 22, 2024
Accepted: June 5, 2024
Published: June 28, 2024

REFERENCES

1. Franks, N.P., and Wisden, W. (2021). The inescapable drive to sleep: Overlapping mechanisms of sleep and sedation. Science *374*, 556–559.
2. Stephan, A.M., Lecci, S., Cataldi, J., and Siclari, F. (2021). Conscious experiences and high-density EEG patterns predicting subjective sleep depth. Curr. Biol. *31*, 5487–5500.e3.
3. Della Monica, C., Johnsen, S., Atzori, G., Groeger, J.A., and Dijk, D.J. (2018). Rapid eye movement sleep, sleep continuity and slow wave sleep as predictors of cognition, mood, and subjective sleep quality in healthy men and women, aged 20-84 years. Front. Psychiatry *9*, 255.
4. Tsai, C.J., Nagata, T., Liu, C.Y., Suganuma, T., Kanda, T., Miyazaki, T., Liu, K., Saitoh, T., Nagase, H., Lazarus, M., et al. (2021). Cerebral capillary blood flow upsurge during REM sleep is mediated by A2a receptors. Cell Rep. *36*, 109558.
5. Nollet, M., Hicks, H., McCarthy, A.P., Wu, H., Möller-Levet, C.S., Laing, E.E., Malki, K., Lawless, N., Wafford, K.A., Dijk, D.J., et al. (2019). REM sleep's unique associations with corticosterone regulation, apoptotic

(E) Schematic illustrating activation of LHb^{Vglut2} neurons using DREADD receptors. *AAV-DIO-hM3Dq-mCherry* was injected into the LHb of *Vglut2-Cre* mice. DG, dentate granule cells; MHb, medial habenula; 3V, third ventricle; scale bar, 100 μm.
(F) Representative traces of EEG/EMG recordings in the saline or CNO-injected groups.
(G) 12 h sleep recording post-saline (black) or CNO (blue) injection. Data are mean ± SEMs.
(H) Summarized changes of sleep duration and latency. Data are mean ± SEMs (n = 7). p values are given when <0.05.
See also Figures S7 and S8.

Please cite this article in press as: Ba et al., A REM-active basal ganglia circuit that regulates anxiety, Current Biology (2024), https://doi.org/10.1016/j.cub.2024.06.010

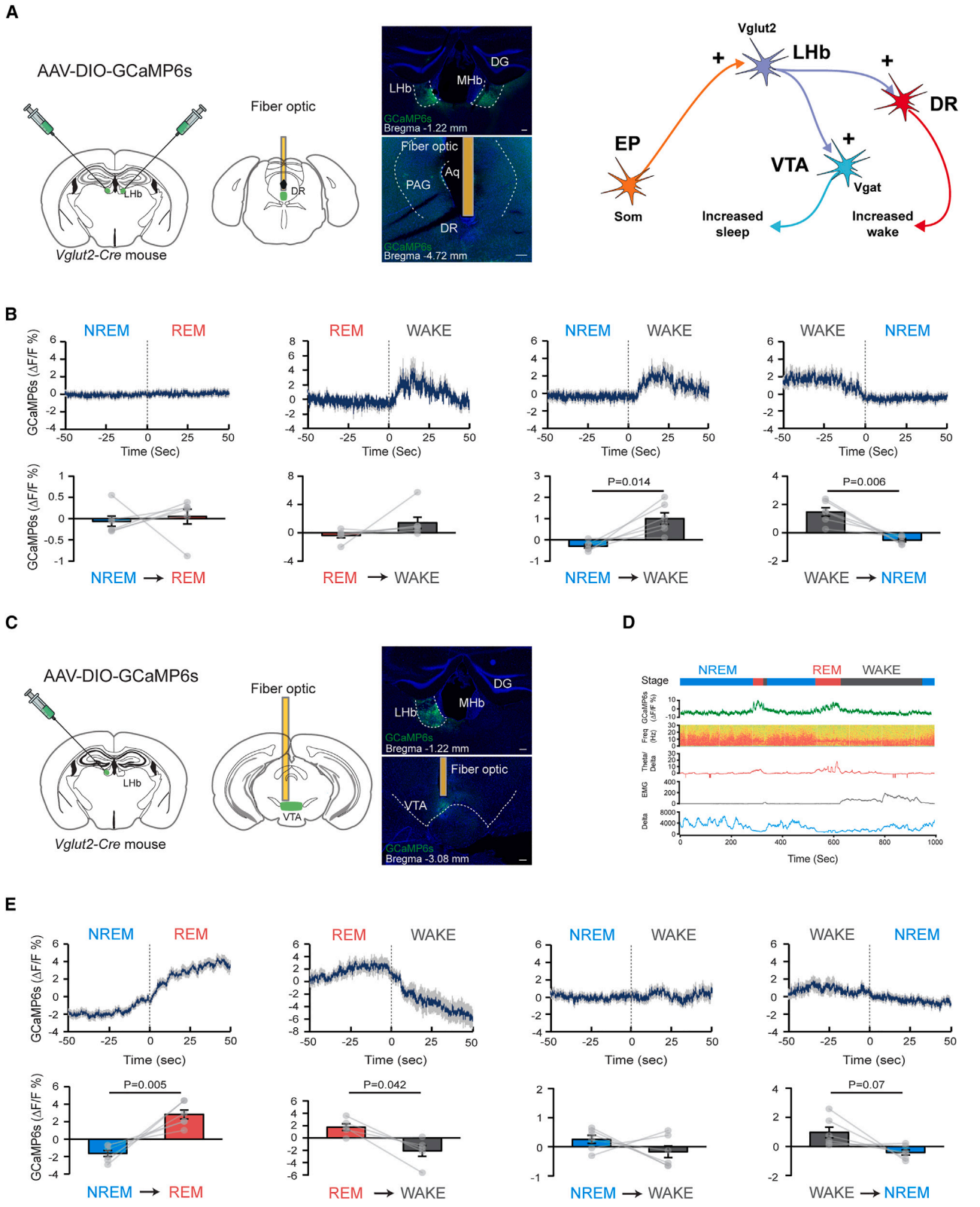

Figure 5. Two downstream targets of the LHb separately drive WAKE and REM sleep

(A) Spontaneous activity across sleep-wake states measured by fiber photometry of LHb terminals in the dorsal raphe (DR) nucleus. Left: schematic illustration of experimental setup; *AAV-DIO-GCaMP6s* was injected into the LHb of *Vglut2-Cre* mice, and a fiber optic was implanted above the DR to record terminal activity.

(legend continued on next page)

pathways, and behavior in chronic stress in mice. Proc. Natl. Acad. Sci. USA *116*, 2733–2742.

6. Wassing, R., Benjamins, J.S., Dekker, K., Moens, S., Spiegelhalder, K., Feige, B., Riemann, D., van der Sluis, S., Van Der Werf, Y.D., Talamini, L.M., et al. (2016). Slow dissolving of emotional distress contributes to hyperarousal. Proc. Natl. Acad. Sci. USA *113*, 2538–2543.
7. Goldstein, A.N., and Walker, M.P. (2014). The role of sleep in emotional brain function. Annu. Rev. Clin. Psychol. *10*, 679–708.
8. Hutchison, I.C., and Rathore, S. (2015). The role of REM sleep theta activity in emotional memory. Front. Psychol. *6*, 1439.
9. Pace-Schott, E.F., Germain, A., and Milad, M.R. (2015). Effects of sleep on memory for conditioned fear and fear extinction. Psychol. Bull. *141*, 835–857.
10. Wassing, R., Lakbila-Kamal, O., Ramautar, J.R., Stoffers, D., Schalkwijk, F., and Van Someren, E.J.W. (2019). Restless REM sleep impedes overnight amygdala adaptation. Curr. Biol. *29*, 2351–2358.e4.
11. Miller, K.E., and Gehrman, P.R. (2019). REM sleep: what is it good for? Curr. Biol. *29*, R806–R807.
12. Murkar, A.L.A., and De Koninck, J. (2018). Consolidative mechanisms of emotional processing in REM sleep and PTSD. Sleep Med. Rev. *41*, 173–184.
13. Simionato, N.M., da Silva Rocha-Lopes, J., Machado, R.B., and Suchecki, D. (2022). Chronic rapid eye movement sleep restriction during juvenility has long-term effects on anxiety-like behaviour and neurotransmission of male Wistar rats. Pharmacol. Biochem. Behav. *217*, 173410.
14. Boyce, R., Glasgow, S.D., Williams, S., and Adamantidis, A. (2016). Causal evidence for the role of REM sleep theta rhythm in contextual memory consolidation. Science *352*, 812–816.
15. Aime, M., Calcini, N., Borsa, M., Campelo, T., Rusterholz, T., Sattin, A., Fellin, T., and Adamantidis, A. (2022). Paradoxical somatodendritic decoupling supports cortical plasticity during REM sleep. Science *376*, 724–730.
16. Izawa, S., Chowdhury, S., Miyazaki, T., Mukai, Y., Ono, D., Inoue, R., Ohmura, Y., Mizoguchi, H., Kimura, K., Yoshioka, M., et al. (2019). REM sleep-active MCH neurons are involved in forgetting hippocampus-dependent memories. Science *365*, 1308–1313.
17. Tseng, Y.T., Zhao, B., Chen, S., Ye, J., Liu, J., Liang, L., Ding, H., Schaefke, B., Yang, Q., Wang, L., et al. (2022). The subthalamic corticotropin-releasing hormone neurons mediate adaptive REM-sleep responses to threat. Neuron *110*, 1223–1239.e8.
18. Palagini, L., Baglioni, C., Ciapparelli, A., Gemignani, A., and Riemann, D. (2013). REM sleep dysregulation in depression: state of the art. Sleep Med. Rev. *17*, 377–390.
19. Kudlow, P.A., Cha, D.S., Lam, R.W., and McIntyre, R.S. (2013). Sleep architecture variation: a mediator of metabolic disturbance in individuals with major depressive disorder. Sleep Med. *14*, 943–949.
20. Riemann, D., Krone, L.B., Wulff, K., and Nissen, C. (2020). Sleep, insomnia, and depression. Neuropsychopharmacology *45*, 74–89.
21. Peever, J., and Fuller, P.M. (2017). The biology of REM sleep. Curr. Biol. *27*, R1237–R1248.
22. Chen, K.S., Xu, M., Zhang, Z., Chang, W.C., Gaj, T., Schaffer, D.V., and Dan, Y. (2018). A hypothalamic switch for REM and non-REM sleep. Neuron *97*, 1168–1176.e4.
23. Luppi, P.H., Billwiller, F., and Fort, P. (2017). Selective activation of a few limbic structures during paradoxical (REM) sleep by the claustrum and the supramammillary nucleus: evidence and function. Curr. Opin. Neurobiol. *44*, 59–64.
24. Renouard, L., Billwiller, F., Ogawa, K., Clément, O., Camargo, N., Abdelkarim, M., Gay, N., Scoté-Blachon, C., Touré, R., Libourel, P.A., et al. (2015). The supramammillary nucleus and the claustrum activate the cortex during REM sleep. Sci. Adv. *1*, e1400177.
25. Gelegen, C., Miracca, G., Ran, M.Z., Harding, E.C., Ye, Z., Yu, X., Tossell, K., Houston, C.M., Yustos, R., Hawkins, E.D., et al. (2018). Excitatory pathways from the lateral habenula enable propofol-induced sedation. Curr. Biol. *28*, 580–587.e5.
26. Stephenson-Jones, M., Yu, K., Ahrens, S., Tucciarone, J.M., van Huijstee, A.N., Mejia, L.A., Penzo, M.A., Tai, L.H., Wilbrecht, L., and Li, B. (2016). A basal ganglia circuit for evaluating action outcomes. Nature *539*, 289–293.
27. Cerniauskas, I., Winterer, J., de Jong, J.W., Lukacsovich, D., Yang, H., Khan, F., Peck, J.R., Obayashi, S.K., Lilascharoen, V., Lim, B.K., et al. (2019). Chronic stress induces activity, synaptic, and transcriptional remodeling of the lateral habenula associated with deficits in motivated behaviors. Neuron *104*, 899–915.e8.
28. Li, H., Pullmann, D., and Jhou, T.C. (2019). Valence-encoding in the lateral habenula arises from the entopeduncular region. eLife *8*, e41223.
29. Hong, S., and Hikosaka, O. (2008). The globus pallidus sends reward-related signals to the lateral habenula. Neuron *60*, 720–729.
30. Hu, H., Cui, Y., and Yang, Y. (2020). Circuits and functions of the lateral habenula in health and in disease. Nat. Rev. Neurosci. *21*, 277–295.
31. Hikosaka, O. (2010). The habenula: from stress evasion to value-based decision-making. Nat. Rev. Neurosci. *11*, 503–513.
32. Gordon-Fennell, A., and Stuber, G.D. (2021). Illuminating subcortical GABAergic and glutamatergic circuits for reward and aversion. Neuropharmacology *198*, 108725.
33. Zhang, L., Hernández, V.S., Swinny, J.D., Verma, A.K., Giesecke, T., Emery, A.C., Mutig, K., Garcia-Segura, L.M., and Eiden, L.E. (2018). A GABAergic cell type in the lateral habenula links hypothalamic homeostatic and midbrain motivation circuits with sex steroid signaling. Transl. Psychiatry *8*, 50.
34. Namboodiri, V.M.K., Rodriguez-Romaguera, J., and Stuber, G.D. (2016). The habenula. Curr. Biol. *26*, R873–R877.
35. Xu, J., Jo, A., DeVries, R.P., Deniz, S., Cherian, S., Sunmola, I., Song, X., Marshall, J.J., Gruner, K.A., Daigle, T.L., et al. (2022). Intersectional mapping of multi-transmitter neurons and other cell types in the brain. Cell Rep. *40*, 111036.
36. Shabel, S.J., Proulx, C.D., Trias, A., Murphy, R.T., and Malinow, R. (2012). Input to the lateral habenula from the basal ganglia is excitatory, aversive, and suppressed by serotonin. Neuron *74*, 475–481.
37. Parent, M., Lévesque, M., and Parent, A. (2001). Two types of projection neurons in the internal pallidum of primates: single-axon tracing and three-dimensional reconstruction. J. Comp. Neurol. *439*, 162–175.

Aq, ventricle; DG, dentate granule cells; MHb, medial habenula; PAG, periaqueductal gray (scale bars, 100 μm). Right: conceptual schematic circuit diagram. EP, entopeduncular nucleus; LHb, lateral habenula; DRN, dorsal raphe nucleus; VTA, ventral tegmental area.

(B) Combined fluorescence responses during transitions between vigilance states for all mice (n = 6). Mean responses of each transition (blue) ± SEM (gray). p values are given when <0.05.

(C) Spontaneous activity measured by fiber photometry across sleep-wake states of LHb terminals in the VTA. Left: schematic illustration of experimental setup. Right: *AAV-DIO-GCaMP6s* was injected into the LHb of *Vglut2-Cre* mice, and a fiber optic was implanted above the VTA to record activity. DG, dentate granule cells; MHb, medial habenula (scale bars, 100 μm).

(D) Representative traces of Ca^{2+} signals aligned with EEG and EMG recordings during wake, NREM, and REM sleep indicated with gray, cyan, and red, respectively.

(E) Combined fluorescence responses during transitions between vigilance states for all mice (n = 6). Mean responses of each transition (blue) ± SEM (gray). p values are given when <0.05.

See also Figures S9–S11.

Please cite this article in press as: Ba et al., A REM-active basal ganglia circuit that regulates anxiety, Current Biology (2024), https://doi.org/10.1016/j.cub.2024.06.010

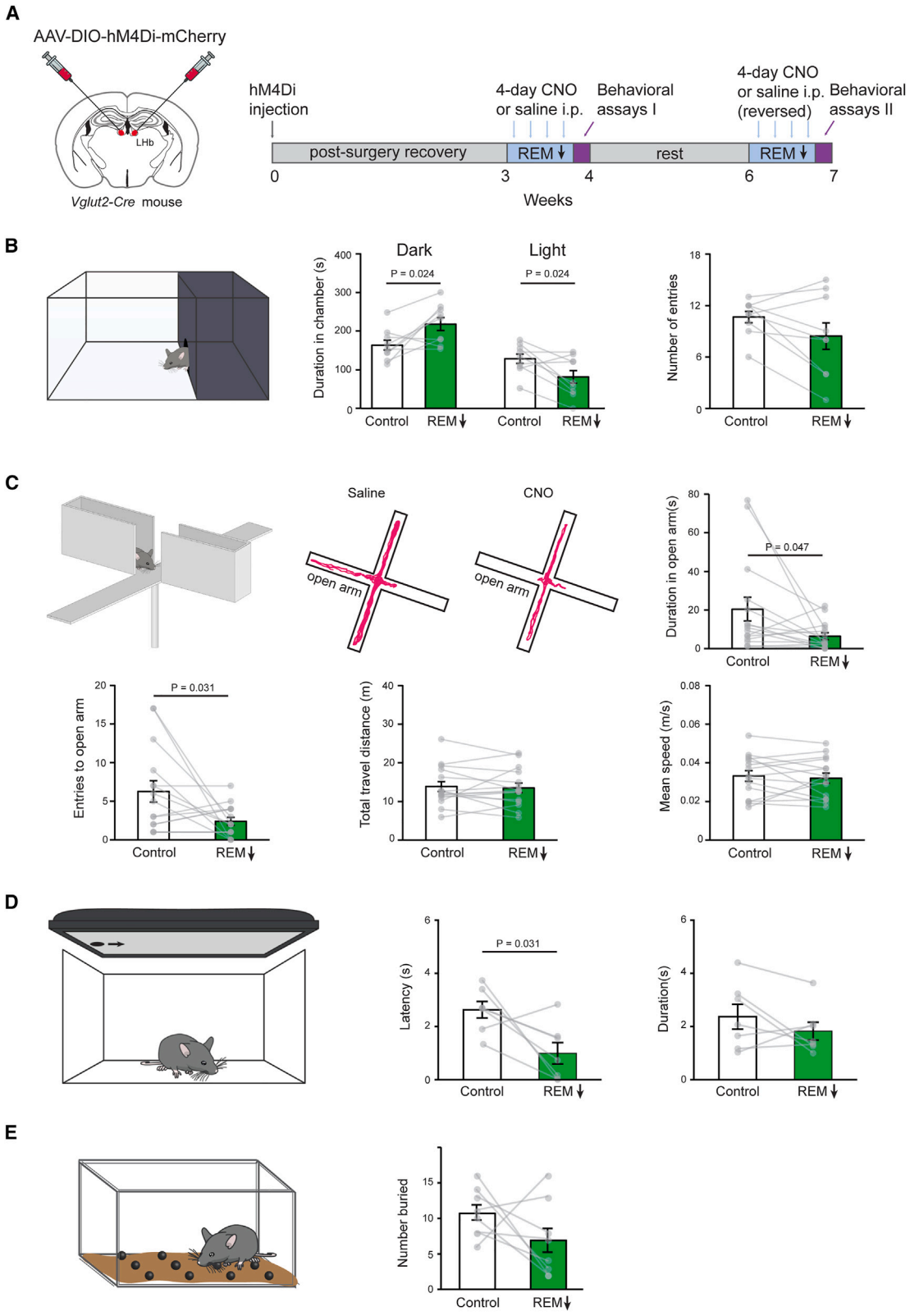

Figure 6. Chronic and selective reduction in REM sleep is accompanied by increased anxiety and altered defensive behavior

(A) Schematic illustration of experimental setup. 3 weeks following transduction of LHb neurons in *Vglut2-Cre* mice with *AAV-DIO-hM4Di-mCherry*, one systemic injection of CNO (1 mg/kg i.p.), or saline, each day for 4 days at the beginning of the light phase caused a cumulative reduction in REM (see Figure S12). Behavioral

(legend continued on next page)

38. Kim, S., Wallace, M.L., El-Rifai, M., Knudsen, A.R., and Sabatini, B.L. (2022). Co-packaging of opposing neurotransmitters in individual synaptic vesicles in the central nervous system. Neuron *110*, 1371–1384.e7.

39. Wallace, M.L., Saunders, A., Huang, K.W., Philson, A.C., Goldman, M., Macosko, E.Z., McCarroll, S.A., and Sabatini, B.L. (2017). Genetically distinct parallel pathways in the entopeduncular nucleus for limbic and sensorimotor output of the basal ganglia. Neuron *94*, 138–152.e5.

40. Hernandez-Martinez, R., and Calakos, N. (2017). Seq-ing the circuit logic of the basal ganglia. Trends Neurosci. *40*, 325–327.

41. Lazaridis, I., Tzortzi, O., Weglage, M., Märtin, A., Xuan, Y., Parent, M., Johansson, Y., Fuzik, J., Fürth, D., Fenno, L.E., et al. (2019). A hypothalamus-habenula circuit controls aversion. Mol. Psychiatry *24*, 1351–1368.

42. Paxinos, G., and Franklin, K.B.J. (2019). Paxinos and Franklin's the Mouse Brain in Stereotaxic Coordinates, Fifth Edition (Elsevier).

43. Yu, X., Li, W., Ma, Y., Tossell, K., Harris, J.J., Harding, E.C., Ba, W., Miracca, G., Wang, D., Li, L., et al. (2019). GABA and glutamate neurons in the VTA regulate sleep and wakefulness. Nat. Neurosci. *22*, 106–119.

44. Oikonomou, G., Altermatt, M., Zhang, R.W., Coughlin, G.M., Montz, C., Gradinaru, V., and Prober, D.A. (2019). The serotonergic raphe promote sleep in zebrafish and mice. Neuron *103*, 686–701.e8.

45. Takahashi, A., Durand-de Cuttoli, R., Flanigan, M.E., Hasegawa, E., Tsunematsu, T., Aleyasin, H., Cherasse, Y., Miya, K., Okada, T., Keino-Masu, K., et al. (2022). Lateral habenula glutamatergic neurons projecting to the dorsal raphe nucleus promote aggressive arousal in mice. Nat. Commun. *13*, 4039.

46. De Franceschi, G., Vivattanasarn, T., Saleem, A.B., and Solomon, S.G. (2016). Vision guides selection of freeze or flight defense strategies in mice. Curr. Biol. *26*, 2150–2154.

47. Luppi, P.H., and Fort, P. (2019). Neuroanatomical and neurochemical bases of vigilance states. Handb. Exp. Pharmacol. *253*, 35–58.

48. Miracca, G., Anuncibay-Soto, B., Tossell, K., Yustos, R., Vyssotski, A.L., Franks, N.P., and Wisden, W. (2022). NMDA receptors in the lateral preoptic hypothalamus are essential for sustaining NREM and REM sleep. J. Neurosci. *42*, 5389–5409.

49. Park, S.H., and Weber, F. (2020). Neural and homeostatic regulation of REM sleep. Front. Psychol. *11*, 1662.

50. Hasegawa, E., Miyasaka, A., Sakurai, K., Cherasse, Y., Li, Y., and Sakurai, T. (2022). Rapid eye movement sleep is initiated by basolateral amygdala dopamine signaling in mice. Science *375*, 994–1000.

51. Oishi, Y., and Lazarus, M. (2017). The control of sleep and wakefulness by mesolimbic dopamine systems. Neurosci. Res. *118*, 66–73.

52. Liu, D., Li, W., Ma, C., Zheng, W., Yao, Y., Tso, C.F., Zhong, P., Chen, X., Song, J.H., Choi, W., et al. (2020). A common hub for sleep and motor control in the substantia nigra. Science *367*, 440–445.

53. Qiu, M.H., Zhong, Z.G., Chen, M.C., and Lu, J. (2019). Nigrostriatal and mesolimbic control of sleep-wake behavior in rat. Brain Struct. Funct. *224*, 2525–2535.

54. Qiu, M.H., Chen, M.C., Wu, J., Nelson, D., and Lu, J. (2016). Deep brain stimulation in the globus pallidus externa promotes sleep. Neuroscience *322*, 115–120.

55. Proulx, C.D., Hikosaka, O., and Malinow, R. (2014). Reward processing by the lateral habenula in normal and depressive behaviors. Nat. Neurosci. *17*, 1146–1152.

56. Szőnyi, A., Zichó, K., Barth, A.M., Gönczi, R.T., Schlingloff, D., Török, B., Sipos, E., Major, A., Bardóczi, Z., Sos, K.E., et al. (2019). Median raphe controls acquisition of negative experience in the mouse. Science *366*, eaay8746.

57. Andalman, A.S., Burns, V.M., Lovett-Barron, M., Broxton, M., Poole, B., Yang, S.J., Grosenick, L., Lerner, T.N., Chen, R., Benster, T., et al. (2019). Neuronal dynamics regulating brain and behavioral state transitions. Cell *177*, 970–985.e20.

58. Wang, R.F., Guo, H., Jiang, S.Y., Liu, Z.L., Qu, W.M., Huang, Z.L., and Wang, L. (2021). Control of wakefulness by lateral hypothalamic glutamatergic neurons in male mice. J. Neurosci. Res. *99*, 1689–1703.

59. Yu, X., Zhao, G., Wang, D., Wang, S., Li, R., Li, A., Wang, H., Nollet, M., Chun, Y.Y., Zhao, T., et al. (2022). A specific circuit in the midbrain detects stress and induces restorative sleep. Science *377*, 63–72.

60. Meye, F.J., Soiza-Reilly, M., Smit, T., Diana, M.A., Schwarz, M.K., and Mameli, M. (2016). Shifted pallidal co-release of GABA and glutamate in habenula drives cocaine withdrawal and relapse. Nat. Neurosci. *19*, 1019–1024.

61. Shabel, S.J., Proulx, C.D., Piriz, J., and Malinow, R. (2014). Mood regulation. GABA/glutamate co-release controls habenula output and is modified by antidepressant treatment. Science *345*, 1494–1498.

62. Yang, Y., Cui, Y., Sang, K., Dong, Y., Ni, Z., Ma, S., and Hu, H. (2018). Ketamine blocks bursting in the lateral habenula to rapidly relieve depression. Nature *554*, 317–322.

63. Vong, L., Ye, C., Yang, Z., Choi, B., Chua, S., Jr., and Lowell, B.B. (2011). Leptin action on GABAergic neurons prevents obesity and reduces inhibitory tone to POMC neurons. Neuron *71*, 142–154.

64. Taniguchi, H., He, M., Wu, P., Kim, S., Paik, R., Sugino, K., Kvitsiani, D., Fu, Y., Lu, J., Lin, Y., et al. (2011). A resource of Cre driver lines for genetic targeting of GABAergic neurons in cerebral cortex. Neuron *71*, 995–1013.

65. Krashes, M.J., Koda, S., Ye, C., Rogan, S.C., Adams, A.C., Cusher, D.S., Maratos-Flier, E., Roth, B.L., and Lowell, B.B. (2011). Rapid, reversible activation of AgRP neurons drives feeding behavior in mice. J. Clin. Invest. *121*, 1424–1428.

66. Chen, T.W., Wardill, T.J., Sun, Y., Pulver, S.R., Renninger, S.L., Baohan, A., Schreiter, E.R., Kerr, R.A., Orger, M.B., Jayaraman, V., et al. (2013). Ultrasensitive fluorescent proteins for imaging neuronal activity. Nature *499*, 295–300.

67. Yang, C.F., Chiang, M.C., Gray, D.C., Prabhakaran, M., Alvarado, M., Juntti, S.A., Unger, E.K., Wells, J.A., and Shah, N.M. (2013). Sexually dimorphic neurons in the ventromedial hypothalamus govern mating in both sexes and aggression in males. Cell *153*, 896–909.

68. Murray, A.J., Sauer, J.F., Riedel, G., McClure, C., Ansel, L., Cheyne, L., Bartos, M., Wisden, W., and Wulff, P. (2011). Parvalbumin-positive CA1 interneurons are required for spatial working but not for reference memory. Nat. Neurosci. *14*, 297–299.

69. Klugmann, M., Symes, C.W., Leichtlein, C.B., Klaussner, B.K., Dunning, J., Fong, D., Young, D., and During, M.J. (2005). AAV-mediated hippocampal

assays were carried out 16 h after the last saline or CNO administration on day 4 following the REM-reduction protocol. After 2 weeks of rest, saline, or CNO (1 mg/kg i.p.), was then again injected i.p. each day for 4 days in a counterbalanced manner followed by a repeat of the behavioral test.

(B) Light/dark box assay. Following REM reduction, mice chose to spend significantly more time in the dark region compared with the light region. The motor activity, as assessed by the number of entries was unchanged. Data are mean ± SEMs. p values are given when <0.05.

(C) In an elevated maze, following REM reduction, mice spent significantly less time in the open arm of the maze, with no change in motor activity. Typical trajectories for a control mouse and one with chronic REM reduction. Mice with REM reduction spent less time and had fewer entries into the open part of the maze, but the total distance traveled and the average speed did not change. Data are mean ± SEMs. p values are given when <0.05.

(D) When presented with a potential looming threat (a black disk moving above them), mice responded by freezing (after a latency interval) and remaining immobile for a certain duration. Following the REM-reduction protocol, the time before freezing (latency) reduced significantly but with no significant change in the duration of immobility. Data are mean ± SEMs. p values are given when <0.05.

(E) REM sleep diminishment did not influence how many marbles mice buried. Data are mean ± SEMs.

See also Figures S12–S14.

expression of short and long Homer 1 proteins differentially affect cognition and seizure activity in adult rats. Mol. Cell. Neurosci. *28*, 347–360.

70. Anisimov, V.N., Herbst, J.A., Abramchuk, A.N., Latanov, A.V., Hahnloser, R.H.R., and Vyssotski, A.L. (2014). Reconstruction of vocal interactions in a group of small songbirds. Nat. Methods *11*, 1135–1137.
71. Alexander, G.M., Rogan, S.C., Abbas, A.I., Armbruster, B.N., Pei, Y., Allen, J.A., Nonneman, R.J., Hartmann, J., Moy, S.S., Nicolelis, M.A., et al. (2009). Remote control of neuronal activity in transgenic mice expressing evolved G protein-coupled receptors. Neuron *63*, 27–39.
72. Gunaydin, L.A., Grosenick, L., Finkelstein, J.C., Kauvar, I.V., Fenno, L.E., Adhikari, A., Lammel, S., Mirzabekov, J.J., Airan, R.D., Zalocusky, K.A., et al. (2014). Natural neural projection dynamics underlying social behavior. Cell *157*, 1535–1551.
73. Yu, X., Ba, W., Zhao, G., Ma, Y., Harding, E.C., Yin, L., Wang, D., Li, H., Zhang, P., Shi, Y., et al. (2021). Dysfunction of ventral tegmental area GABA neurons causes mania-like behavior. Mol. Psychiatry *26*, 5213–5228.
74. Felix-Ortiz, A.C., Burgos-Robles, A., Bhagat, N.D., Leppla, C.A., and Tye, K.M. (2016). Bidirectional modulation of anxiety-related and social behaviors by amygdala projections to the medial prefrontal cortex. Neuroscience *321*, 197–209.
75. Thomas, A., Burant, A., Bui, N., Graham, D., Yuva-Paylor, L.A., and Paylor, R. (2009). Marble burying reflects a repetitive and perseverative behavior more than novelty-induced anxiety. Psychopharmacol. (Berl.) *204*, 361–373.

Please cite this article in press as: Ba et al., A REM-active basal ganglia circuit that regulates anxiety, Current Biology (2024), https://doi.org/10.1016/j.cub.2024.06.010

CellPress
OPEN ACCESS

STAR★METHODS

KEY RESOURCES TABLE

REAGENT or RESOURCE	SOURCE	IDENTIFIER
Antibodies		
Rabbit polyclonal anti-cFOS	Sigma-Aldrich	Cat# ABE457; RRID:AB_2631318
Rat monoclonal mCherry	Thermo Fisher Scientific	Cat# M11217; RRID: AB_2536611
Chicken polyclonal GFP	Abcam	Cat# ab13970; RRID: AB_300798
Rabbit polyclonal somatostation	Abcam	Cat# ab108456; RRID: AB_11158517
Mouse monoclonal tyrosine hydroxylase	Merck	Cat# T2928; RRID: AB_477569
Alexa Fluor 488 goat anti-rabbit	Invitrogen	Cat# A11108; RRID:AB_143165
Alexa Fluor 488 goat anti-mouse	Invitrogen	Cat# A11001; RRID: AB_2534069
Alexa Fluor 594 goat anti-mouse	Invitrogen	Cat# A11005; RRID: AB_2534073
Alexa Fluor 594 goat anti-rabbit	Invitrogen	Cat# A11037; RRID: AB_2534095
Alexa Fluor 594 goat anti-rat	Invitrogen	Cat# A11007; RRID: AB_10561522
Alexa Fluor 647 goat anti-mouse	Invitrogen	Cat# A-21235; RRID: AB_2535804
Bacterial and virus strains		
Adenovirus helper plasmid *pFΔ6*	Donated by M Klugmann	N/A
AAV helper plasmid *pH21* (AAV1)	Donated by M Klugmann	N/A
AAV helper plasmid pRVI(AAV2)	Donated by M Klugmann	N/A
pAAV-hSyn-DIO-hM3Dq-mCherry	Gift from Bryan L. Roth	Addgene plasmid 44361
pAAV-hSyn-DIO-hM4Di-mCherry	Gift from Bryan L. Roth	Addgene plasmid 44362
pAAV-hSyn-DIO-GCaMP6s	Addgene	Addgene plasmid 184284
pGP-CMV-GCaMP6s	Addgene	Addgene plasmid 40753
pAAV-EF1α-DIO-taCASP3-TEV	Gift from Nirao Shah	Addgene plasmid 45580
pAAV-EF1α-flex-hChR2(H314R)-EYFP	Addgene	Addgene plasmid 20298
Chemicals, peptides, and recombinant proteins		
Clozapine-N-oxide	Sigma-Aldrich	C0832
Hoechst 33342	Thermo Fisher Scientific	H3507
Experimental models: Organisms/strains		
Mouse: *Vglut2-ires-Cre* (*Slc17a6*$^{tm2(cre)Lowl}$/*J*)	Jackson Lab	JAX Stock 016963
Mouse: *Vgat-ires-Cre* (*Slc32a1*$^{tm2(cre)Lowl}$/*J*)	Jackson Lab	JAX Stock 016962
Mouse: *Som-ires-Cre* (*Sst* $^{tm2.1(cre)Zjh}$/*J*)	Jackson Lab	JAX Stock 013044
Software and algorithms		
Spike 2	This paper	https://ced.co.uk/products/spkovin
Matlab	This paper	https://uk.mathworks.com/
Fiji	N/A	https://fiji.sc/

RESOURCE AVAILABILITY

Lead contact

Further information and requests for resources and reagents should be directed to and will be fulfilled by the lead contact and corresponding authors: Nicholas P. Franks or William Wisden (n.franks@imperial.ac.uk, w.wisden@imperial.ac.uk).

Materials availability

This study did not generate new unique reagents.

Data and code availability

- All data reported in this paper will be shared by the lead contact upon request.
- This paper does not report original code.
- Any additional information required to reanalyze the data reported in this paper is available from the lead contact upon request.

EXPERIMENTAL MODEL AND STUDY PARTICIPANT DETAILS

All procedures were approved by the Animal Welfare Ethical Review Body at Imperial College London. Experiments were performed in accordance with the UK Home Office Animal Procedures Act (1986). *Vglut2-ires-Cre* mice (*Slc17a6*$^{tm2(cre)Lowl}$/*J*) and *Vgat-ires-Cre* mice (*Slc32a1*$^{tm2(cre)Lowl}$/*J*) were kindly provided by B.B. Lowell (JAX lab stock 016963 and JAX lab stock 016962)[63]; *Som-ires-Cre* mice (*Sst* $^{tm2.1(cre)Zjh}$/*J* (JAX lab stock 013044) were kindly donated by Z. J. Huang.[64]

Mice were housed at constant temperature (22 ± 1 °C), humidity and circadian cycle (reversed 12 h light-dark cycle). Food and water were available *ad libitum*. Both male and female heterozygous mice 10–12 weeks of age at the start of experimental procedures were used in all experiments.

METHOD DETAILS

Viral constructs and preparation

Cre-inducible recombinant AAV vectors carrying transgenes encoding chemogenetic receptors (*pAAV-hSyn-DIO-hM3Dq-mCherry* and *pAAV-hSyn-DIO-hM4Di-mCherry*) were gifts from Bryan L. Roth (Addgene plasmids 44361 and 44362)[65]; for optogenetics, *pAAV-EF1α-DIO-hChR2(H314R)-EYFP* was a gift from Karl Deisseroth (Addgene plasmid 20298). For calcium photometry experiments, plasmid *pAAV-hSyn-DIO-GCaMP6s* (Addgene plasmid 184284) was generated by inserting the *GCaMP6s* open reading frame from *pGP-CMV-GCaMP6s* (Addgene plasmid 40753, gift of Douglas Kim)[66] into the *pAAV-hSyn-DIO-hM3Dq-mCherry* backbone, as we described previously.[43] For the caspase lesions, *pAAV-EF1α-DIO-taCASP3-TEV* was a gift from Nirao Shah (Addgene plasmid 45580).[67] All vectors were packed into AAV capsids in-house (mixed 1:1 ratio of AAV1 and AAV2 capsids proteins with AAV2 ITRs) as described previously.[68,69] Aliquots of virus were stored at -80 °C before stereotaxic injection.

Stereotaxic surgery

Mice were anesthetized with isoflurane (induced at 4% and maintained at 1.5% - 2.5%) in oxygen (vol/vol) and positioned on a stereotaxic frame (Angle Two, Leica Microsystems, Milton Keynes, Buckinghamshire, UK). A heat pad was used during the surgery to prevent heat loss (ThermoStar, RWD Life Sciences). A digital mouse brain atlas was linked to the injection frame guide the desired brain regions. The following coordinates were used: for LHb: AP = -1.7 mm; ML = ±0.4 mm; DV = -2.6 mm; for EP: AP = -1.22 mm; ML ±1.77 mm; DV -4.64 mm; for VTA: AP = -3.52 mm; ML -0.36 mm; DV -4.3 mm; for DRN: AP = −4.6 mm; ML = 0.00 mm; DV = −4.64 mm. The virus (0.2 μl – 0.3 μl total volume depending on the viral titer) was injected through a stainless steel 33-gauge/15mm/PST3 internal cannula (Hamilton) attached to a 10 μl Hamilton syringe, at a rate of 0.1 μl min^{-1}. After infusion, the cannula was left at the injection site for five minutes and then slowly withdrawn.

For photometry recordings, following AAV injection, a mono-fiber optic cannula (200 μm; Doric Lenses, Inc., Quebec, Canada) was placed 100 μm above the EP, LHb, VTA or DRN. The cannula was affixed with a M1 screw and with dental cement. For locally infusing saline or CNO in the VTA, guide cannulas were implanted above VTA. We conducted post-mortem analysis to verify the viral injection sites and to evaluate the placement of the fiber optic or guide cannulas. Only mice with appropriate viral expression pattern and fibre/cannula implantation were included in this study.

EEG and EMG recording and scoring of sleep-wake behaviors

Non-tethered EEG and EMG recordings were captured using Neurologger 2A device as described previously.[70] Mice were implanted with three miniature screw electrodes (–1.5 mm Bregma, +1.5 mm midline, first recording electrode; +1.5 mm Bregma, –1.5 mm midline, second recording electrode; –1 mm Lambda, 0 mm midline, reference electrode) with two EMG wires inserted in the dorsal neck muscles (AS634, Cooner Wire, CA). The EEG-EMG device was affixed to the skull with Orthodontic Resin power and Orthodontic resin liquid (Tocdental, UK). All mice were allowed 3-4 weeks for recovery in their home cages. Data were recorded with four times oversampling at a sampling rate of 200 Hz. Collected data was downloaded and waveforms visualized using Spike2 software (Cambridge Electronic Design, Cambridge, UK). The EEG signals were high-pass filtered (0.5 Hz, -3dB, an FFT size of 512 was the designated time window) using a digital filter. The EMG signals were band-pass filtered between 5-45 Hz (-3dB). Power in the delta (0.5-4 Hz), theta (6-10 Hz) bands and theta to delta band ratio were calculated, along with the root mean square (RMS) value of the EMG signal (averaged over a bin size of 5 s). All of these data were used to define the vigilance states of WAKE, NREM and REM by an automatic script. Each vigilance state was screened and confirmed manually afterward. The peak frequency during NREM epochs were analyzed using Fourier transform power spectra to average power spectra over blocks of time.

For chemogenetic experiments,[71] clozapine-N-oxide (C0832, Sigma-Aldrich, dissolved in saline, 1 mg/kg) or saline was injected *i.p.* and the vigilance states were recorded. Mice were split into random groups that received either saline or CNO injection. After

conducting preliminary experiments, for the hM3-expressing mice, CNO or saline were injected during the "lights off" active phase; for the hM4-expressing mice, CNO or saline were injected at the start of the "lights on" sleep phase.

For local chemogenetic activation experiments, CNO (3 μM, 0.2 μl) or saline (0.2 μl) was unilaterally infused via a guided cannula over 5 min and sleep-wake states were recorded simultaneously.

For optogenetic experiments, *Som-Cre* mice injected with *AAV-DIO-ChR2-EYFP* or *AAV-DIO-GFP* were tethered to an optic fiber patch cable (Ø 200 μm, 0.22 numerical aperture, Doric Lenses). Open-loop stimulation was used by repeatedly delivering 20 Hz pulse trains (10 ms) for 120 s every 30 min, generated by a blue 473 nm laser (1 mW, Shanghai Laser & Optics Century Co.). Sleep-wake states were recorded and compared before and after the stimulation.

Immunohistochemistry

Mice were deeply anesthetized with an overdose of pentobarbital (100 mg/kg body weight; i.p.) and transcardially perfused with 4% paraformaldehyde (Thermo Scientific) in phosphate buffered saline (PBS, pH 7.4, Sigma-Aldrich). After post-fixation overnight, the mouse brain was preserved in 30% sucrose/PBS for 2 days. 60-μm-thick coronal sections were sliced using a Leica SM 2010R microtome. Free-floating sections were washed in PBS three times for 5 min, permeabilized in PBS plus 0.4% Triton X-100 for 15 min (for somatostatin staining, 2 hours of permeabilization using 0.3 % Triton X-100 was used) and blocked by incubation in PBS plus 5% normal goat serum (NGS) (Vector), 0.2% Triton X-100 for 1 hour. Sections were incubated with primary antibody diluted in PBS plus 2% NGS overnight at 4°C in a shaker. Incubated slices were then washed three times in PBS for 10 min, and incubated for 2 hours with secondary antibody (Molecular Probes) in PBS and subsequently washed three times in PBS for 10 min (all at room temperature). Before mounting, slices were incubated with Hoechst 33342 (Thermo Fisher Scientific) for 15min followed by rinsing with PBS. Finally, slices were mounted on slides, embedded in Dako mounting medium (Agilent Technologies) and imaged using an inverted wide-field microscope (Zeiss Axio Observer) or a Leica SP5 MP confocal microscope (Facility for Imaging by Light Microscopy, FILM, Imperial College London).

Primary antibodies used were rabbit polyclonal cFos (1:4000, Sigma-Aldrich); rat monoclonal mCherry (1:2000, Thermo Fisher Scientific); chicken polyclonal GFP (1:1000, Abcam); and rabbit polyclonal somatostatin (1:100, Abcam); mouse monoclonal tyrosine hydroxylase (1:1000, Merck), secondary antibodies were Alexa Fluor 488 goat anti-rabbit, Alexa Fluor 488 goat anti-mouse, Alexa Fluor 594 goat anti-rabbit, Alexa Fluor 594 goat anti-mouse (1:1000, Invitrogen Molecular Probes, UK).

Fiber photometry

To determine the spontaneous activity of targeted neurons during baseline sleep, we used fiber photometry as previously described.[43,72] Briefly, we used a 473-nm diode-pumped solid-state blue laser for GCaMP6s excitation (Shanghai Laser & Optics Century Co.). The laser light was passed through a single-source fluorescence cube (FMC_GFP_FC, Doric Lenses) through an optical fiber patch cord (Ø 200 μm, 0.22 numerical aperture, Doric Lenses). From the filter cube, a multimodal optical patch cord (Ø 200 μm, 0.37 numerical aperture) was attached to a ceramic optical fiber (Ø 200 μm, 0.37 numerical aperture) implanted into the mouse brain with a ceramic split mating sleeve ferrule (Thorlabs). The GCaMP6 output was then filtered at 500–550 nm using a second dichroic in the fluorescence cube and converted to voltage by an amplified photodiode (APD-FC, Doric Lenses). The photodiode signal was output to a lock-in amplifier (SR810, Stanford Research Systems) and the power of the laser was set to 80 μW at the fiber tip. The signal was then digitized using a CED 1401 Micro Box (Cambridge Electronic Design) and recorded at 1 kHz using Spike2 software (Cambridge Electronic Design).

The photometry signal was aligned with the EEG and EMG recordings. For each experiment, the photometry signal F was normalized to the baseline signal using $\Delta F/F(t) = (F(t) - \text{median (F)})/\text{median } (F)$.[43] We observed a decay of photometry signal at the beginning of some recordings. All the sessions were selected after the photometry signal became stable. We performed the recordings in 2–3 sessions per mouse, one session for 6 h. For the transitions for vigilance states, several sessions were randomly chosen and analyzed.

Behavioral Tests

To evaluate the behavioral changes after 4-day REM sleep restriction, we used several assays. All mice were handled daily by the experimenter for 5 minutes for 3 days before the start of the experiments. On the day of testing, mice were transferred to the testing room 30 min prior to the experiment. All behavior tests were performed during the dark phase.

Light/dark box assay

The arena (36 (l) x 27 (w) x 30 cm (h), Zantiks LT system) is divided into one dark "safe" compartment (one third) and one large illuminated light compartment (two thirds) with a 50 mm semi-circle hole allowing mice to move freely between the two compartments. Mice were placed in the dark side of the arena and movement was tracked for 5 min by an overhead video camera positioned above the arena. The number of transitions as well as the time spent in each compartment were calculated.

Elevated plus maze assay

This was performed as we previously described.[73] The elevated plus maze (Ugo Basile) was made of grey non-reflective plastic and consisted of two open arms (35 x 5 cm) and two enclosed arms (35 x 5 x 15 cm) extending from a central platform at 90 degrees in the form of a plus. The maze was elevated 60 cm from the floor. Individual mice were placed in the center and allowed 5 minutes to explore the maze. The movements were captured and tracked with an overhead video camera. Time spent in each arm, speed and travel distance were calculated using Any-maze software (Stoelting). For acute optogentic excitation experiments, we used a

9 min test session with three 3-min epochs to involve additional within-subject and within-session comparations, as described before.[74]

Looming test

We adopted a previously reported protocol.[46] Briefly, the test was performed in a 48 x 35 x 30 cm arena. The loom stimulus was a 2.5 cm black disk generated using Raspberry Pi. The stimuli were presented on one side of an LCD monitor displaying a grey screen and smoothly moved to the opposite side over 4s. Videos of mouse movements were recorded and processed in MATLAB with a home-made script.

Marble burying test

New cages with equal amount of bedding were filled with 20 glass marbles (15-mm diameter) in a 4 x 5 arrangement. Mice were transferred from home cages and allowed to explore the new cages for 20 min. The number of marbles buried (> 2/3 covered by bedding material) was recorded and compared.[75]

QUANTIFICATION AND STATISTICAL ANALYSIS

Mice with an incorrect viral expression or fiber/cannula placement were excluded from the analysis. Analyses were performed with GraphPad Prism 8 (GraphPad software) and MATLAB (Mathworks). Data are presented as the mean ± SEM. We used either two-tailed or paired t-test for data that were not independent. *P*-values are shown when they were <0.05.

Current Biology, Volume *34*

Supplemental Information

A REM-active basal ganglia circuit that regulates anxiety

Wei Ba, Mathieu Nollet, Chunyu Yin, Xiao Yu, Sara Wong, Andawei Miao, Esteban J. Beckwith, Edward C. Harding, Ying Ma, Raquel Yustos, Alexei L. Vyssotski, William Wisden, and Nicholas P. Franks

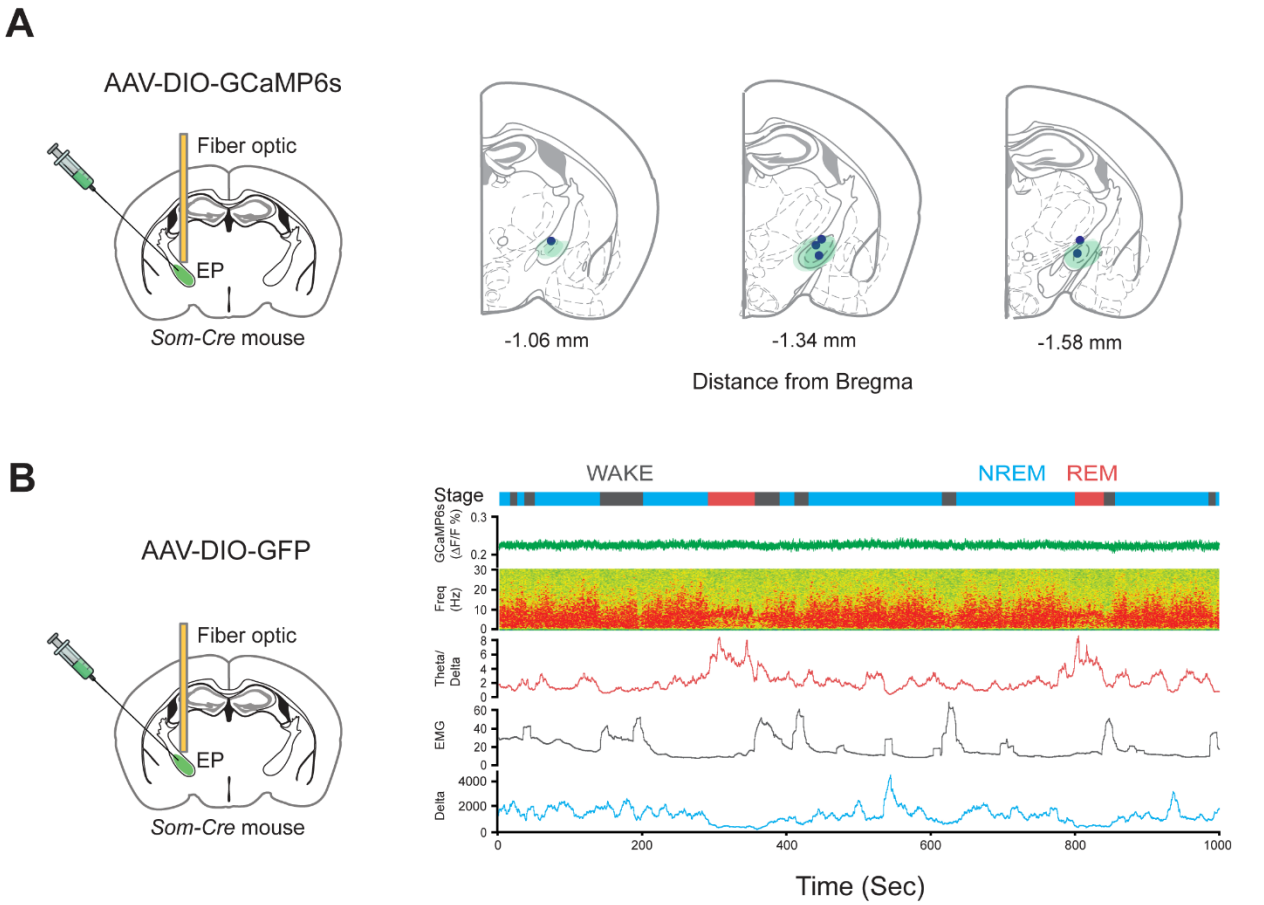

Figure S1 Histological verification and controls for EP photometry recordings. Related to Figure 1.

(A) Confirmation of viral injection and optic fiber implantation. Green, areas transduced with *AAV-DIO-GCaMP6s*; Blue, location of optic fiber placement. (B) Schematic of the photometry recordings on *Som-Cre* mice injected with *AAV-DIO-GFP* control and representative traces aligned with EEG/EMG recordings. (C) Quantification of the Ca^{2+} signal showed no vigilance state-dependent activity. Data are means ± SEMs.

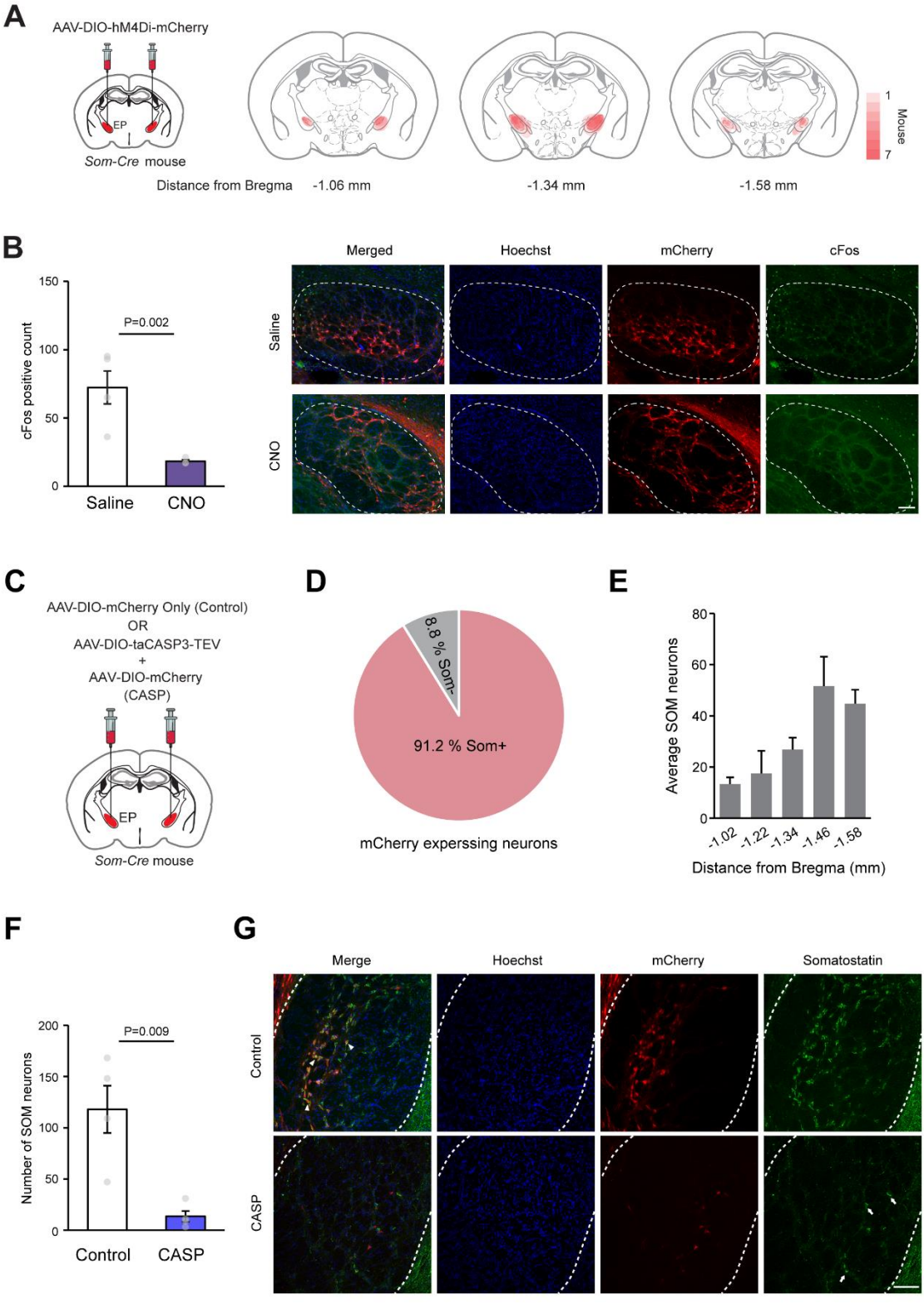
A
AAV-DIO-hM4Di-mCherry
EP
Som-Cre mouse
Distance from Bregma -1.06 mm
-1.34 mm
-1.58 mm
1
Mouse
7
B
cFos positive count
150
100
50
0
P=0.002
Saline
CNO
Merged
Hoechst
mCherry
cFos
Saline
CNO
C
AAV-DIO-mCherry Only (Control)
OR
AAV-DIO-taCASP3-TEV
+
AAV-DIO-mCherry
(CASP)
EP
Som-Cre mouse
D
8.8 % Som-
91.2 % Som+
mCherry experssing neurons
E
Average SOM neurons
80
60
40
20
0
-1.02
-1.22
-1.34
-1.46
-1.58
Distance from Bregma (mm)
F
Number of SOM neurons
200
150
100
50
0
P=0.009
Control
CASP
G
Merge
Hoechst
mCherry
Somatostatin
Control
CASP

Figure S2 Verification of hM4Di and caspase-mediated ablation. Related to Figure 2.

(A) Confirmation of the expression of *AAV-DIO-hM4Di-mCherry* in the EP. (B) Validation of the inhibitory effect of hM4Di on cFOS expression in the EP. Left, quantification of cFOS in the EP in the saline control and CNO injected groups; Right, representative images showing cFOS expression in the EP ($P = 0.002$, $n = 3$). (C) Experimental strategy of EP^{Som} lesioning. Bilateral injection of *AAV-DIO-mCherry* only (control) or combined *AAV-DIO-mCherry* and *AAV-DIO-CASP3* into the EP of *Som-Cre* mice. (D) The percentage of control mCherry expressing neurons co-labelled with somatostatin antibodies. (E) Distribution of somatostatin neurons in the EP. (F) Number of EP^{Som} neurons in the control and CASP groups. (G) Representative images show mCherry expression (red) and EP^{Som} neurons (green) as determined by immunohistochemistry ($P = 0.009$, $n = 3$). Arrowheads show mCherry and somatostatin double positive EP neurons; arrows indicate survived EP^{Som} neurons after lesioning. Scale bars, 100 μm. All data are means ± SEMs; *P* values are given when <0.05.

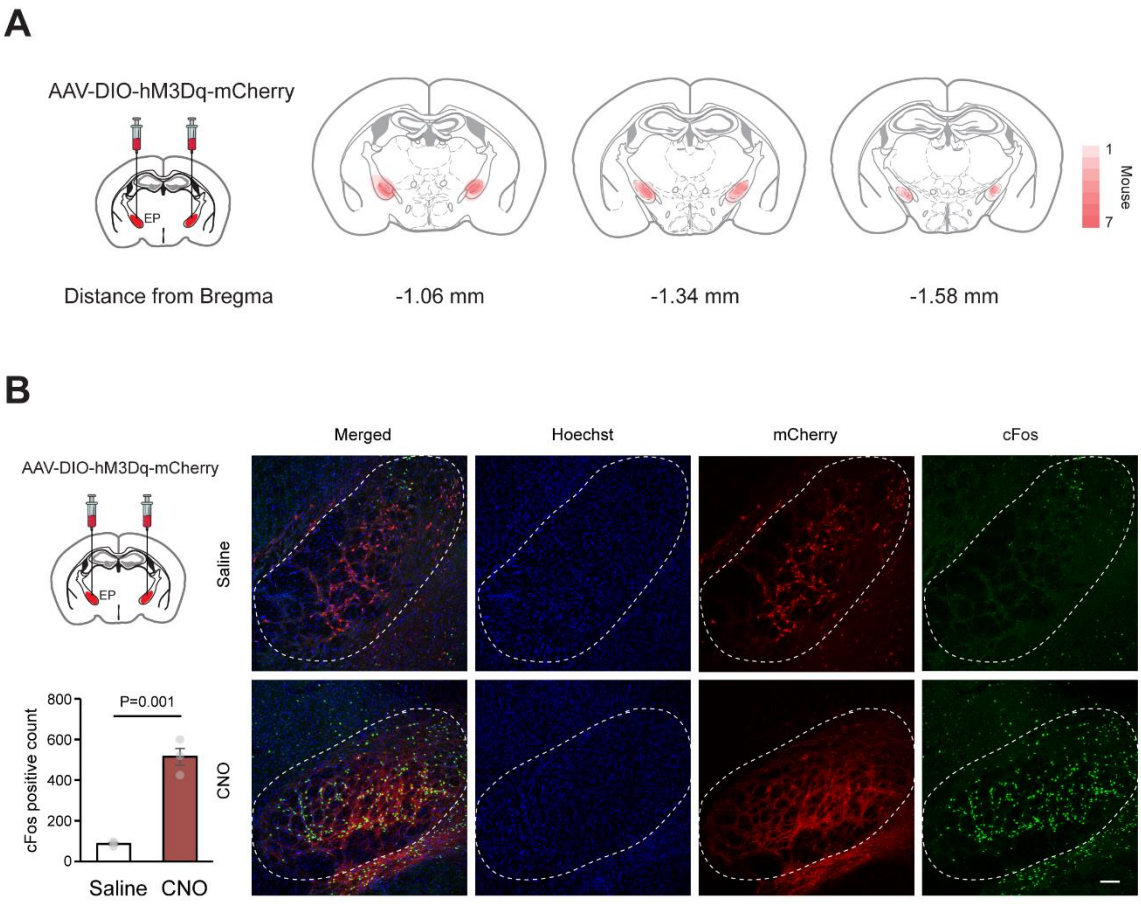

Figure S3 Verification of viral expression and activation of hM3Dq. Related to Figure 2.

(A) Histological confirmation of *AAV-DIO-hM3Dq-mCherry*. (B) Quantification and representative images showing increased cFOS expression after CNO injection in the EP (P = 0.001, n = 3). Scale bar, 100 μm. Data are means ± SEMs; P values are given when <0.05.

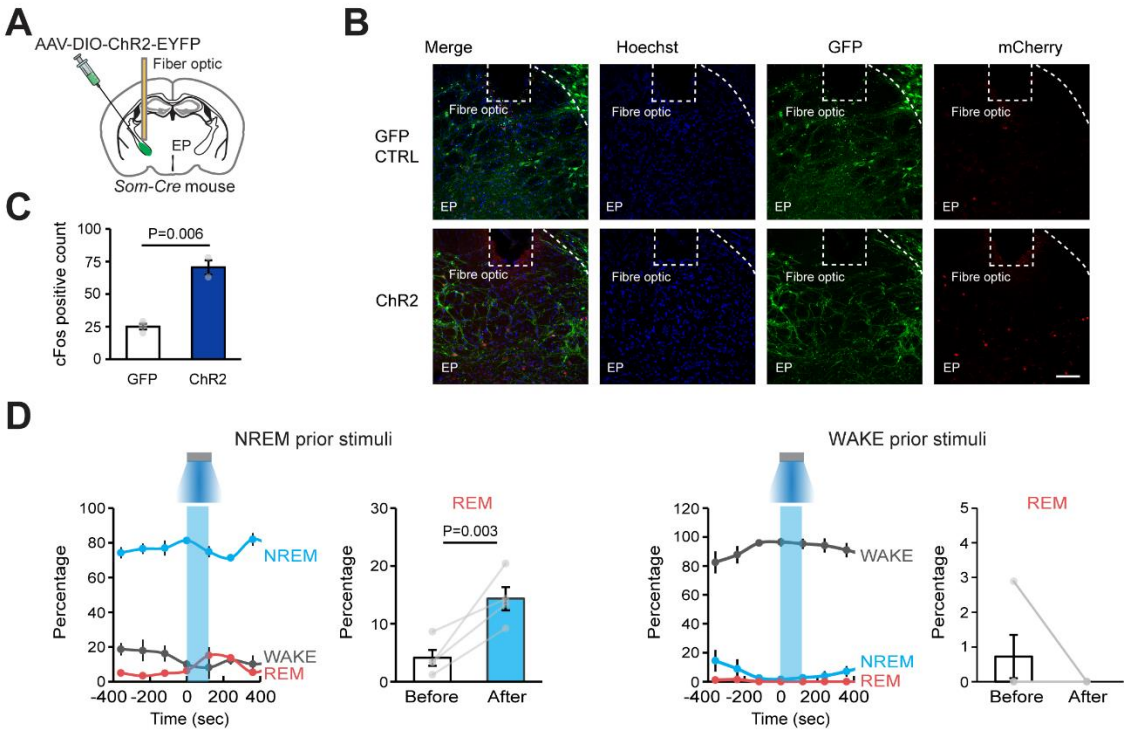

Figure S4 Optogenetic activation of EP^{Som} neurons during NREM sleep induces REM sleep. Related to Figure 2.

(A-C) Effects of laser stimulation on cFOS expression in mice expressing GFP or ChR2-EYFP in EP^{Som} cells. (A) Experimental setting for optogenetic stimulation. (B-C) cFos expression in the EP following laser stimulation (*n* = 3). (D) Changes in sleep-wake states after laser stimulation. Mean percentage of each stage when laser was turned on during NREM sleep (left) or WAKE (right) (*n* = 4). All data are means ± SEMs; *P* values are given when <0.05.

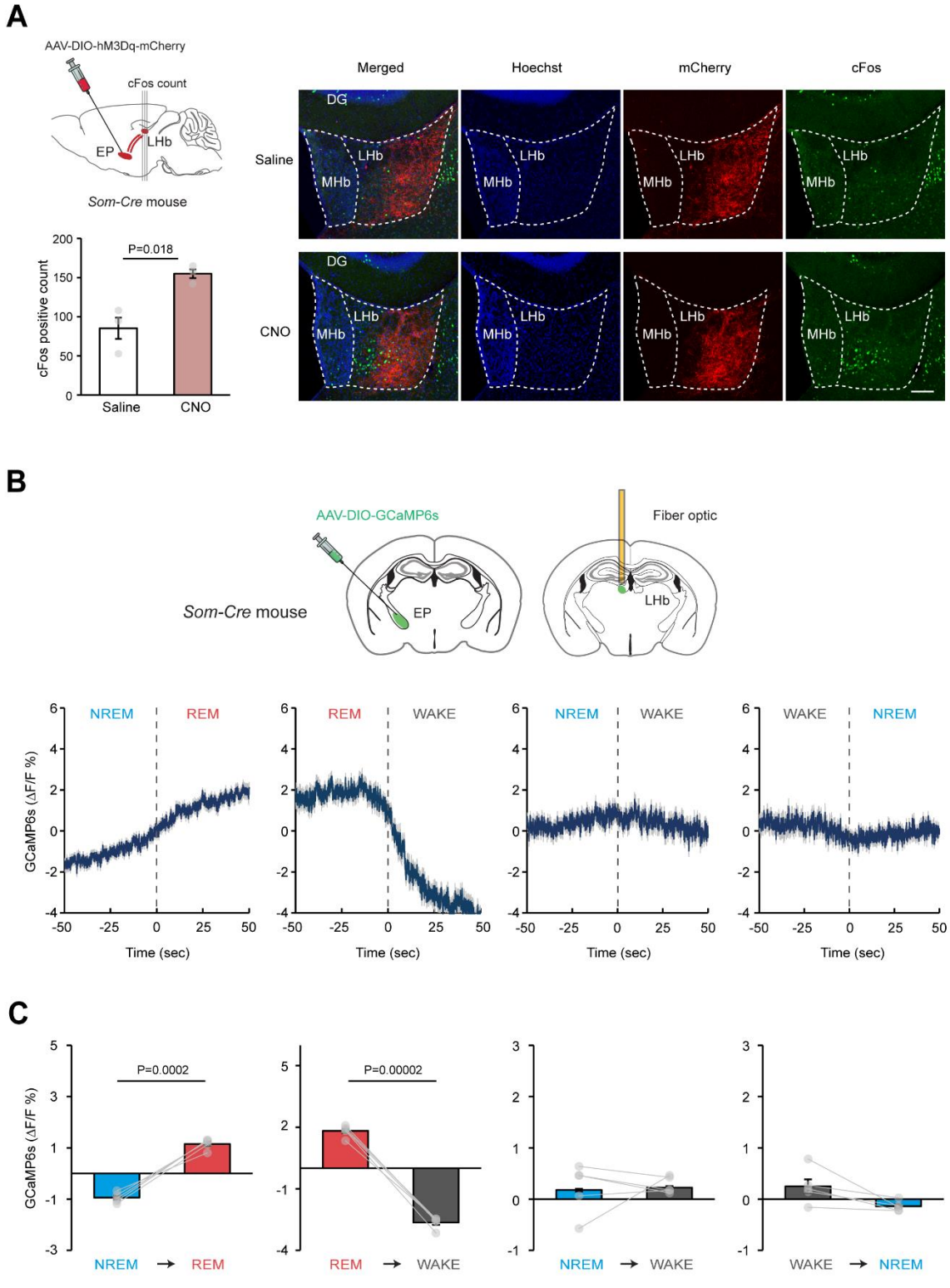
A
AAV-DIO-hM3Dq-mCherry
cFos count
EP
LHb
Som-Cre mouse
Merged
Hoechst
mCherry
cFos
Saline
CNO
DG
LHb
MHb
cFos positive count
P=0.018
Saline
CNO
B
AAV-DIO-GCaMP6s
Fiber optic
Som-Cre mouse
EP
LHb
NREM
REM
WAKE
GCaMP6s (ΔF/F %)
Time (sec)
C
P=0.0002
P=0.00002
NREM → REM
REM → WAKE
NREM → WAKE
WAKE → NREM

Figure S5 EP^{Som} terminals in the LHb are active during REM, mirroring activity in the EP soma. Related to Figure 3.

(A) Evaluation of cFos expression in the LHb upon the activation of EP^{Som} neurons. Top left, experimental design, Right, representative pictures showing the EP^{Som} terminals (red) and cFos (green) in the LHb, Bottom left, quantification of cFos positive neurons (*n* = 3). (B) *AAV-DIO-GCaMP6s* was injected in EP^{Som} neurons of *Som-Cre* mice and an optical fiber was positioned over the LHb. The Ca^{2+} transients at EP→LHb terminals peaked during REM sleep. NREM-REM transitions were associated with prominent increases of activity at these terminals. (C) Summary of transitions between states. All data are means ± SEMs; *P* values are given when <0.05.

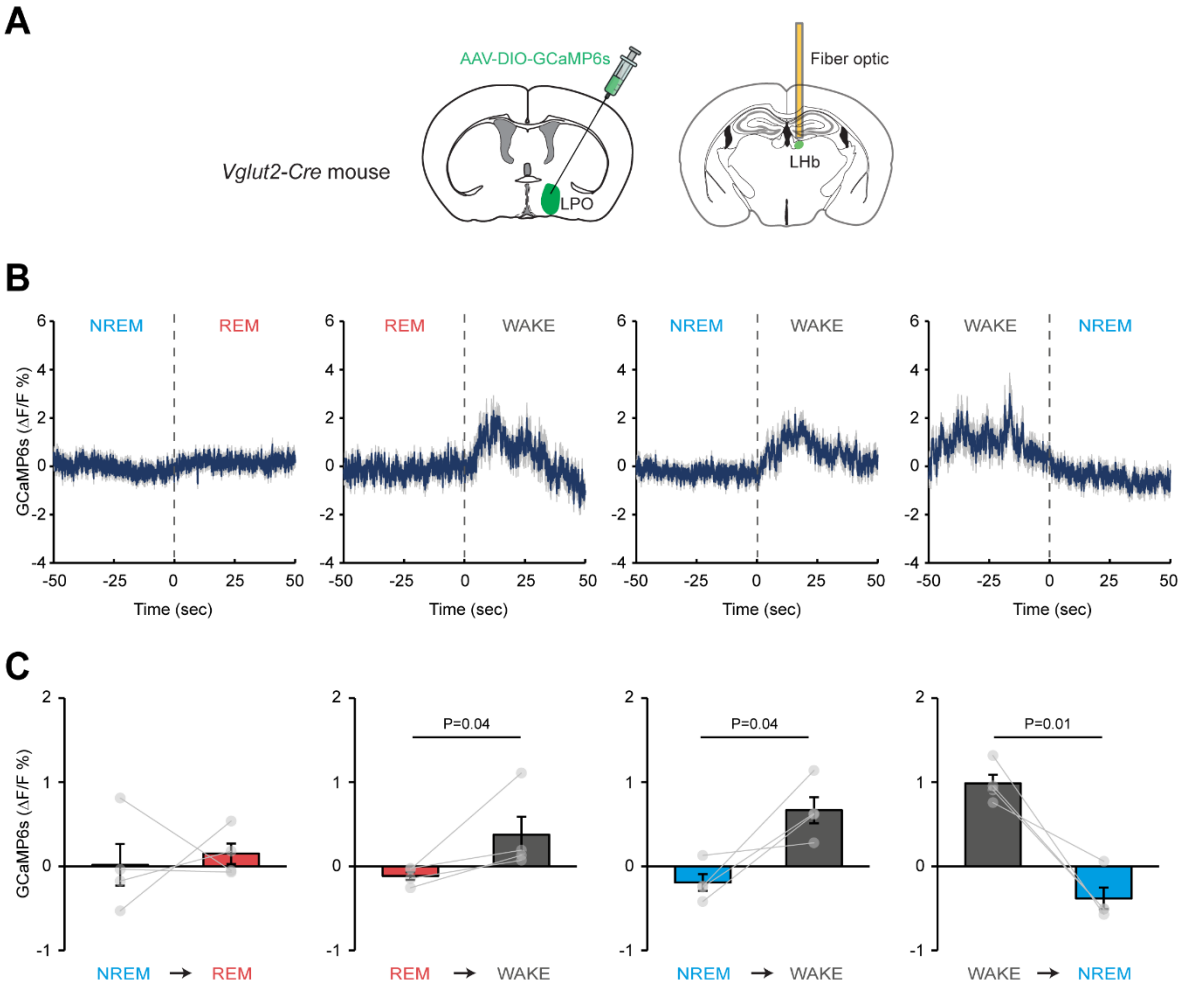

Figure S6 Glutamatergic LPO terminals in the LHb are selectively WAKE-active. Related to Figure 3.

(A) *AAV-DIO-GCaMP6s* was transduced in LPO^{Vglut2} neurons of *Vglut2-Cre* mice and an optical fiber positioned over the LHb. (B) Combined fluorescence responses during transitions between vigilance states for all mice. The Ca^{2+} transients at LPO→LHb terminals were highest during wakefulness. (C) Summary of transitions between states. All data are means ± SEMs; *P* values are given when <0.05.

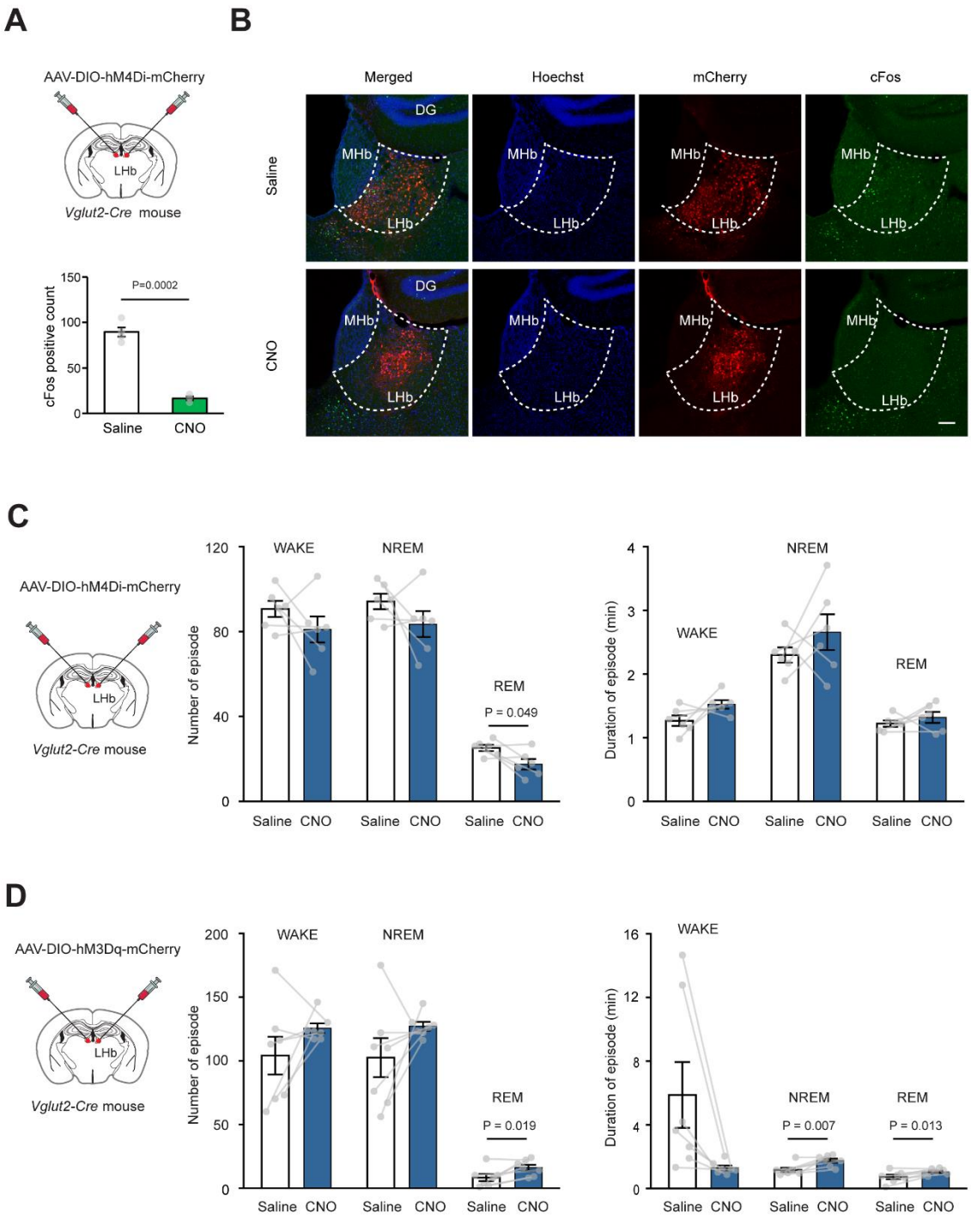
A
AAV-DIO-hM4Di-mCherry
LHb
Vglut2-Cre mouse
cFos positive count
P=0.0002
Saline
CNO
B
Merged
Hoechst
mCherry
cFos
Saline
CNO
DG
MHb
LHb
C
AAV-DIO-hM4Di-mCherry
Vglut2-Cre mouse
Number of episode
WAKE
NREM
REM
P = 0.049
Duration of episode (min)
D
AAV-DIO-hM3Dq-mCherry
Vglut2-Cre mouse
P = 0.019
P = 0.007
P = 0.013

Figure S7 Validation of hM4Di in the LHb and detailed analysis of sleep during activation and inhibition of LHb^{Vglut2} neurons. Related to Figure 4.

(A-B) Validation of hM4Di in the LHb. (A) Top left, experimental design. *AAV-DIO-hM4Di-mCherry* was bilaterally injected into the LHb of *Vglut2-Cre* mice. Bottom left, quantification of cFOS positive cells. CNO injection reduced the number of cFOS in the LHb. (B) Representative images of mCherry (red) and cFOS (green) expression in both saline and CNO groups. (C-D) Analysis of sleep episodes. (C) CNO-mediated inhibition of LHb^{Vglut2} neurons decreased REM sleep by decreasing the number of REM episodes (n = 7). (D) *AAV-DIO-hM3Dq-mCherry* was bilaterally injected into the LHb of *Vglut2-Cre* mice. CNO-mediated excitation of LHb^{Vglut2} neurons increased REM sleep by increasing the number of REM episodes and increasing their durations. The duration of NREM episodes also increased (n = 7). In both groups of mice, CNO was injected *i.p.* at 1 mg/kg. All data are means ± SEMs; P values are given when <0.05.

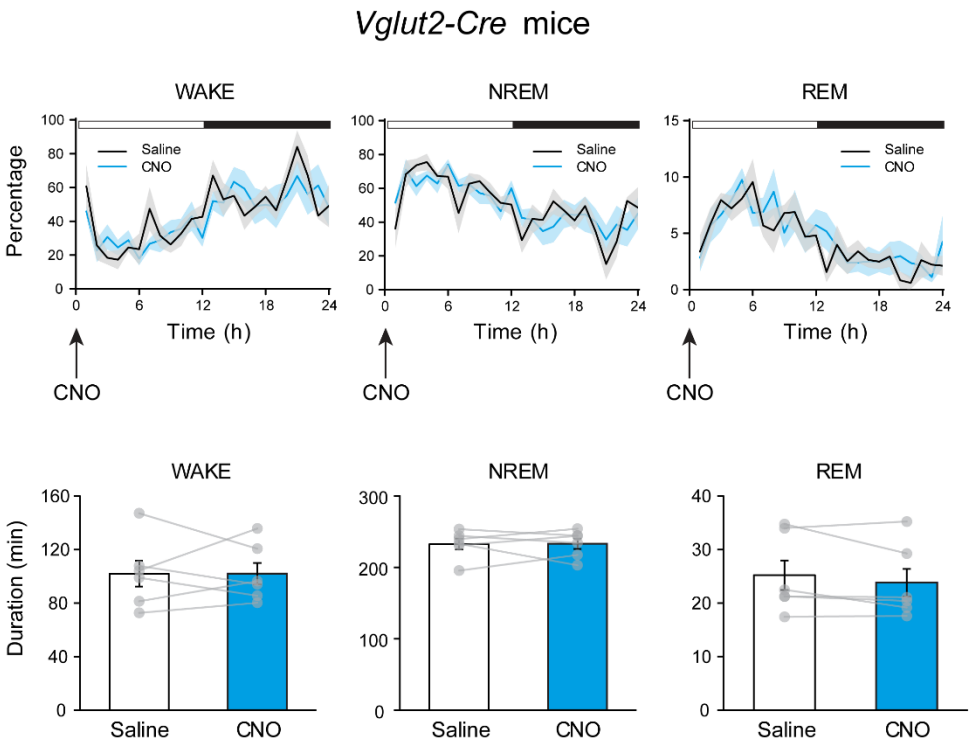

Figure S8 CNO (1 mg/kg; *i.p.*) have no effect on vigilance states in *Vglut2-Cre* mice. Related to Figure 4.

Following *i.p.* injection, CNO at 1 mg/kg had no effect on the amounts of WAKE, NREM or REM sleep over the following 24 hours compared with mice injected with saline (n = 6). Data are means ± SEMs.

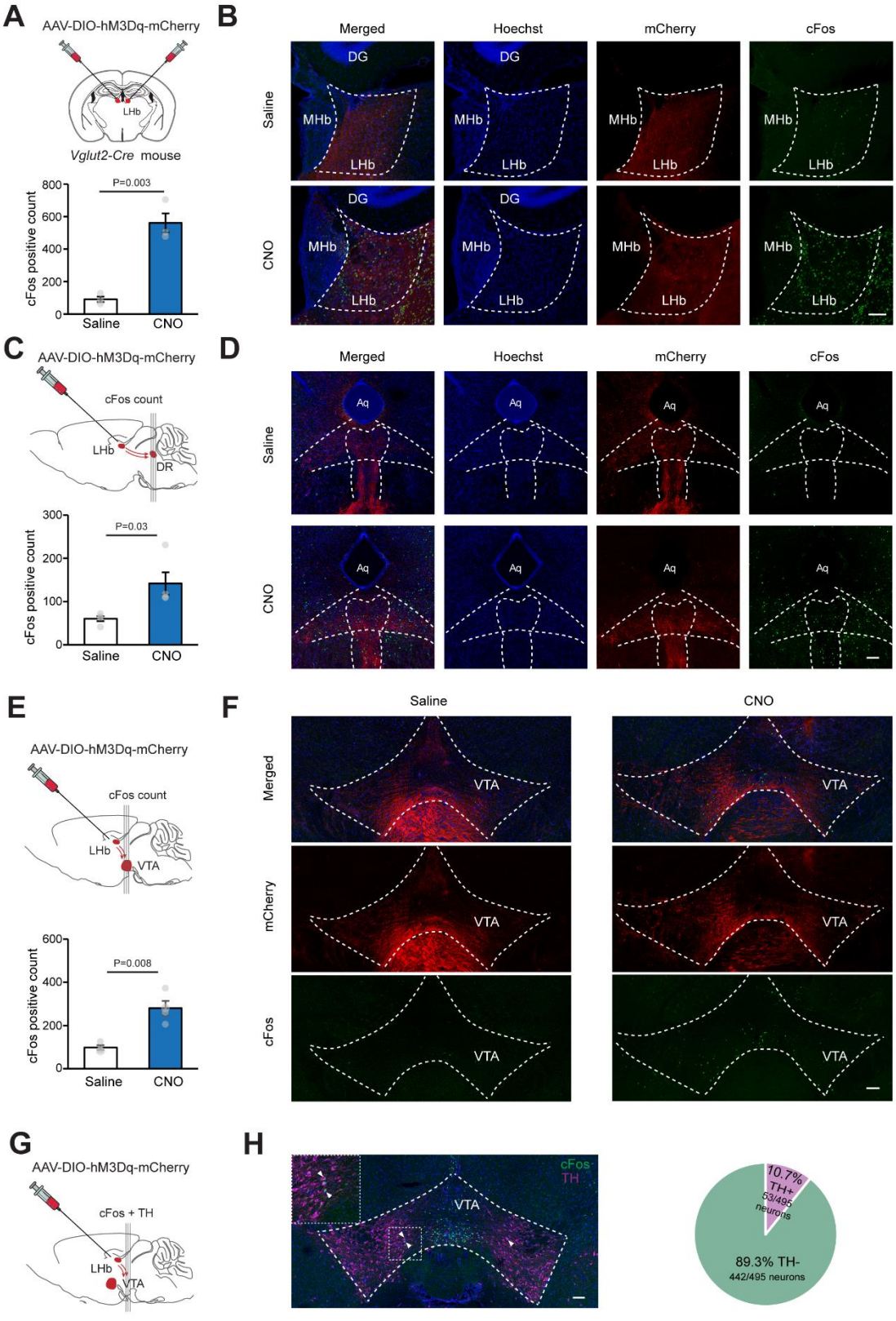
A
AAV-DIO-hM3Dq-mCherry
LHb
Vglut2-Cre mouse
cFos positive count
P=0.003
Saline
CNO
B
Merged
Hoechst
mCherry
cFos
Saline
CNO
DG
MHb
LHb
C
AAV-DIO-hM3Dq-mCherry
cFos count
LHb
DR
cFos positive count
P=0.03
Saline
CNO
D
Merged
Hoechst
mCherry
cFos
Saline
CNO
Aq
E
AAV-DIO-hM3Dq-mCherry
cFos count
LHb
VTA
cFos positive count
P=0.008
Saline
CNO
F
Saline
CNO
Merged
mCherry
cFos
VTA
G
AAV-DIO-hM3Dq-mCherry
cFos + TH
LHb
VTA
H
cFos
TH
VTA
10.7% TH+
53/495 neurons
89.3% TH-
442/495 neurons

Figure S9 Chemogenetically activating glutamatergic cells in the LHb increased cFos expression in the downstream DRN and VTA circuitry. Related to Figure 5.
(A-B) CNO administration successfully activated glutamatergic neurons in the LHb, as determined by cFOS expression. (A) Top, experimental setup. *AAV-DIO-hM3Dq-mCherry* was injected into the LHb of *Vglut2-Cre* mice; Bottom, the number of cFos-expressing cells was increased after CNO injection (*n* = 3). (B) Representative images showing expression of hM3Dq in the somata of the LHb (red) and cFos staining (green). (C-D) Excitation of LHb^{Vglut2} neurons induced cFos expression in the downstream DRN. (C) Top, schematic of the experimental design; Bottom, quantification of cFos in the saline and CNO group (*n* = 3). (D) Representative pictures of the LHb axons (red) and cFos staining (green) in the DRN. (E-F) Activating LHb^{Vglut2} neurons increased cFos-positive neurons in a downstream target, the VTA. (E) Top, schematic of the experimental setup; Bottom, quantification of cFos expression in the VTA (*n* = 3). Scale bars, 100 μm. (G-H) Evaluation of the percentage of activated VTA dopaminergic neurons upon LHb excitation. (G) Experimental settings. (H) Staining and quantification cFOS and tyrosine hydroxylase (TH) double positive neurons. Arrowheads indicate cFOS and TH double positive neruons. All data are means ± SEMs; *P* values are given when <0.05.

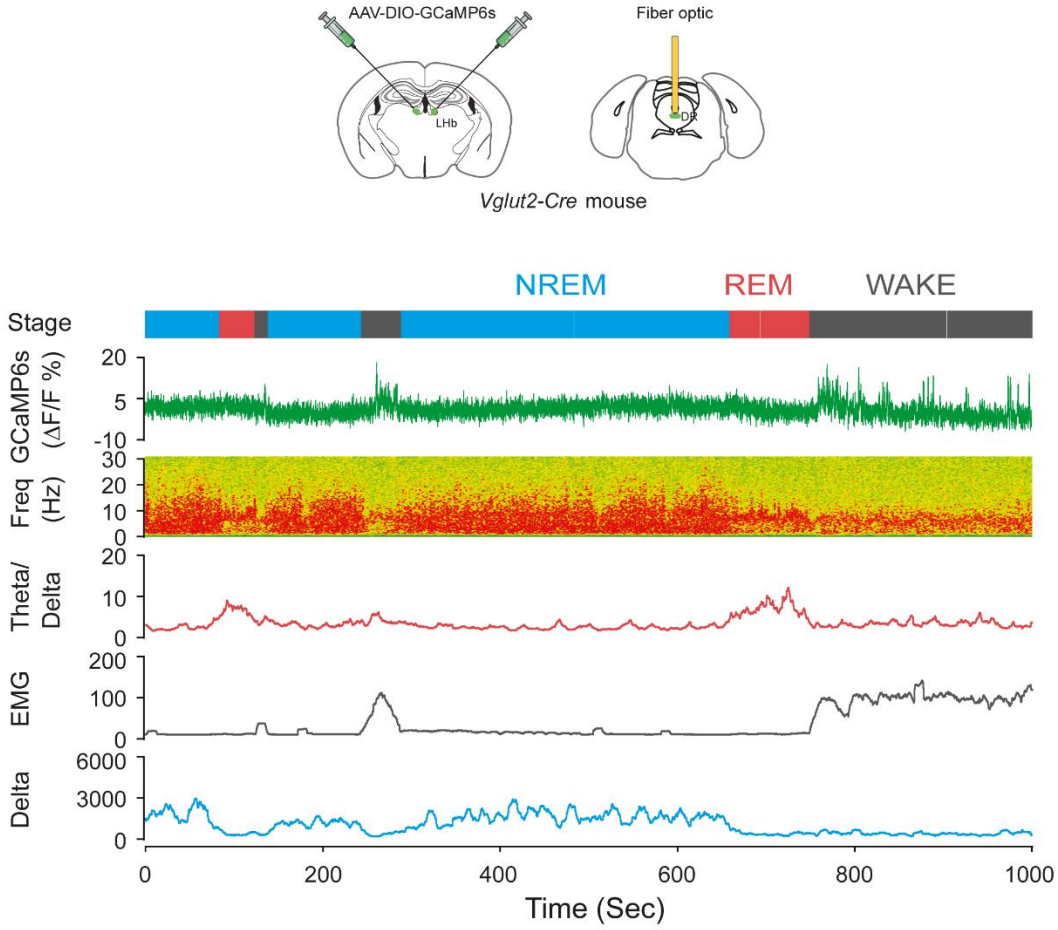

Figure S10 Representative traces of Ca^{2+} signals in the LHb terminals in the dorsal raphe aligned with EEG and EMG recordings during wakefulness, NREM and REM sleep showing increased activity during WAKE. Related to Figure 5.

Representative fiber photometry recordings at LHb→DRN terminals across sleep-wake cycles were achieved by expressing *AAV-DIO-GCaMP6s* in LHb^{Vglut2} neurons and with optical fibers placed over terminals in the dorsal raphe (DR).

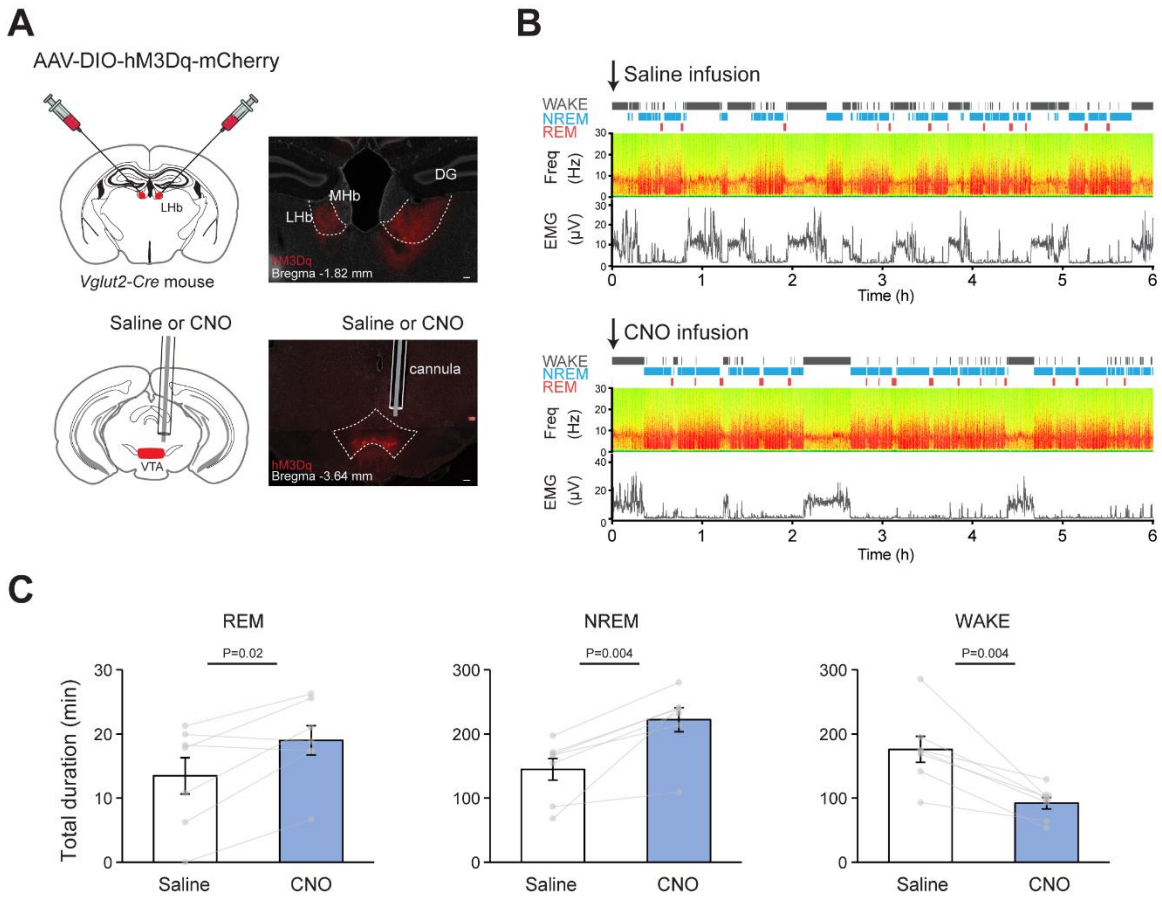

Figure S11 Local chemogenetic activation of LHb^{Vglut2} terminals in the VTA neurons increases REM and NREM sleep. Related to Figure 5.

(A) Excitation of LHb^{Vglut2} terminals in the VTA using hM3Dq-mCherry receptors. *AAV-DIO-hM3Dq-mCherry* was injected into the LHb of *Vglut2-Cre* mice. A guided cannula was placed in the VTA to locally infuse saline or CNO. Immunostaining confirmed the expression of hM3Dq-mCherry in the LHb soma and terminals in the VTA as well as the placement of the guided cannula. (Scale bars, 100 μm.) (B) Representative EEG/EMG recordings post-saline or CNO local infusion into the VTA. (C) Summarized changes on WAKE, NREM and REM duration. Data are means ± SEMs (*n* = 7); *P* values are given when <0.05.

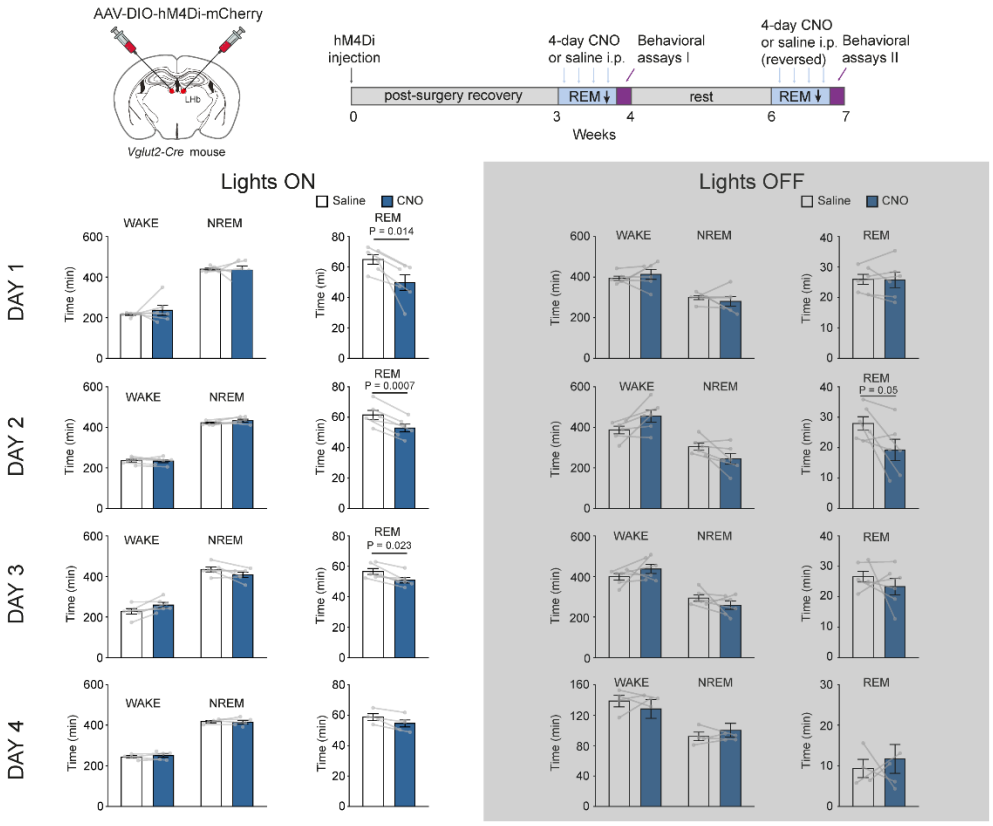

Figure S12 Repeated inhibition of LHb^{Vglut2} neurons by CNO caused a reduction in REM. Related to Figure 6.

Vglut2-Cre mice were injected bilaterally into the lateral habenula (LHb) with *AAV-DIO-hM4Di-mCherry*. Prior to behavioral assays, the percentage of REM was reduced by repeated (once per day for 4 days) injections of CNO (1 mg/kg) at the beginning of the light phase in LHb^{Vglut2} mice. All data are means ± SEMs; *P* values are given when <0.05.

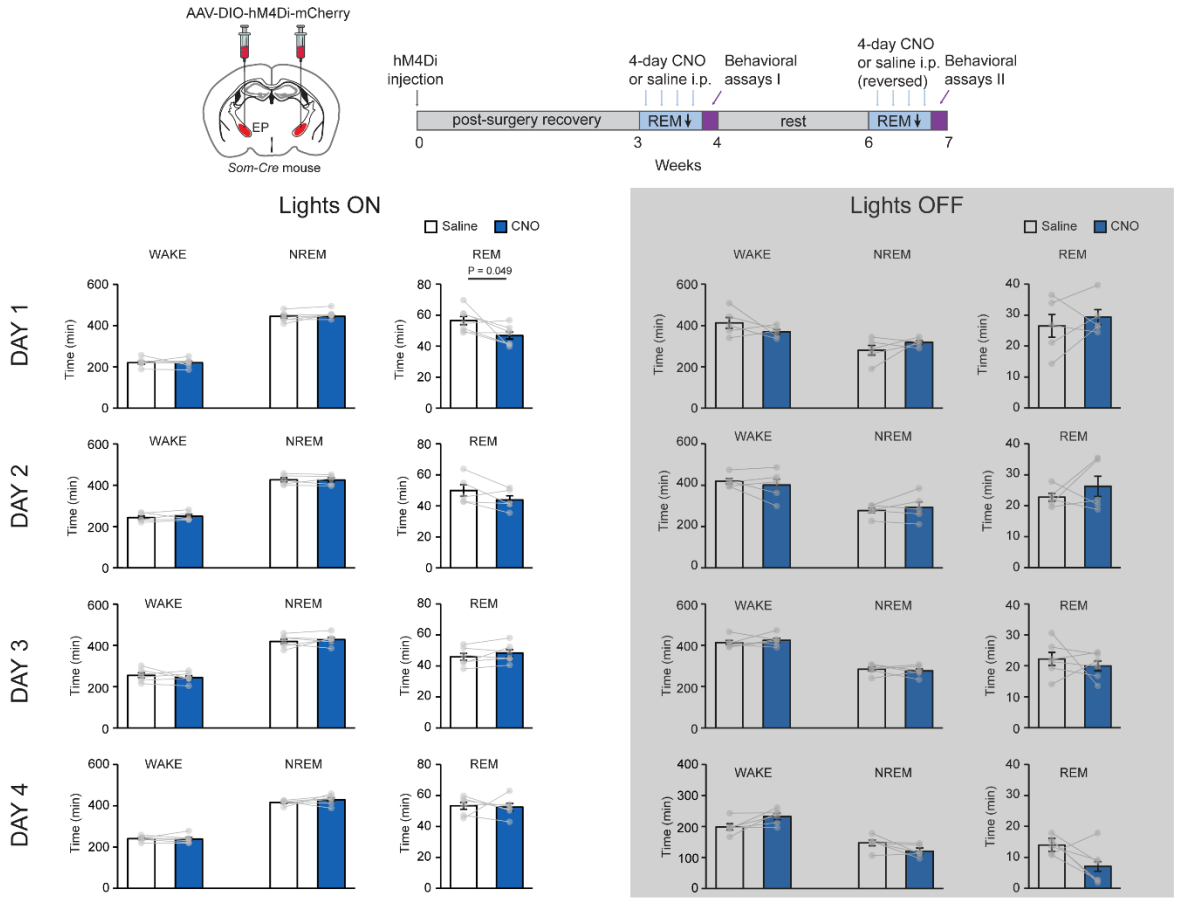

Figure S13. Repeated inhibition of EP^{Som} neurons by CNO caused a reduction in REM on Day1 of the treatment but not subsequent days. Related to Figure 6.
Som-Cre mice were injected bilaterally into the EP with *AAV-DIO-hM4Di-mCherry.* Prior to the behavioral assays shown in Figure S14, mice received repeated (once per day for 4 days) injections of saline or CNO (1 mg/kg) at the start of the light phase. All data are means ± SEMs; *P* values are given when <0.05.

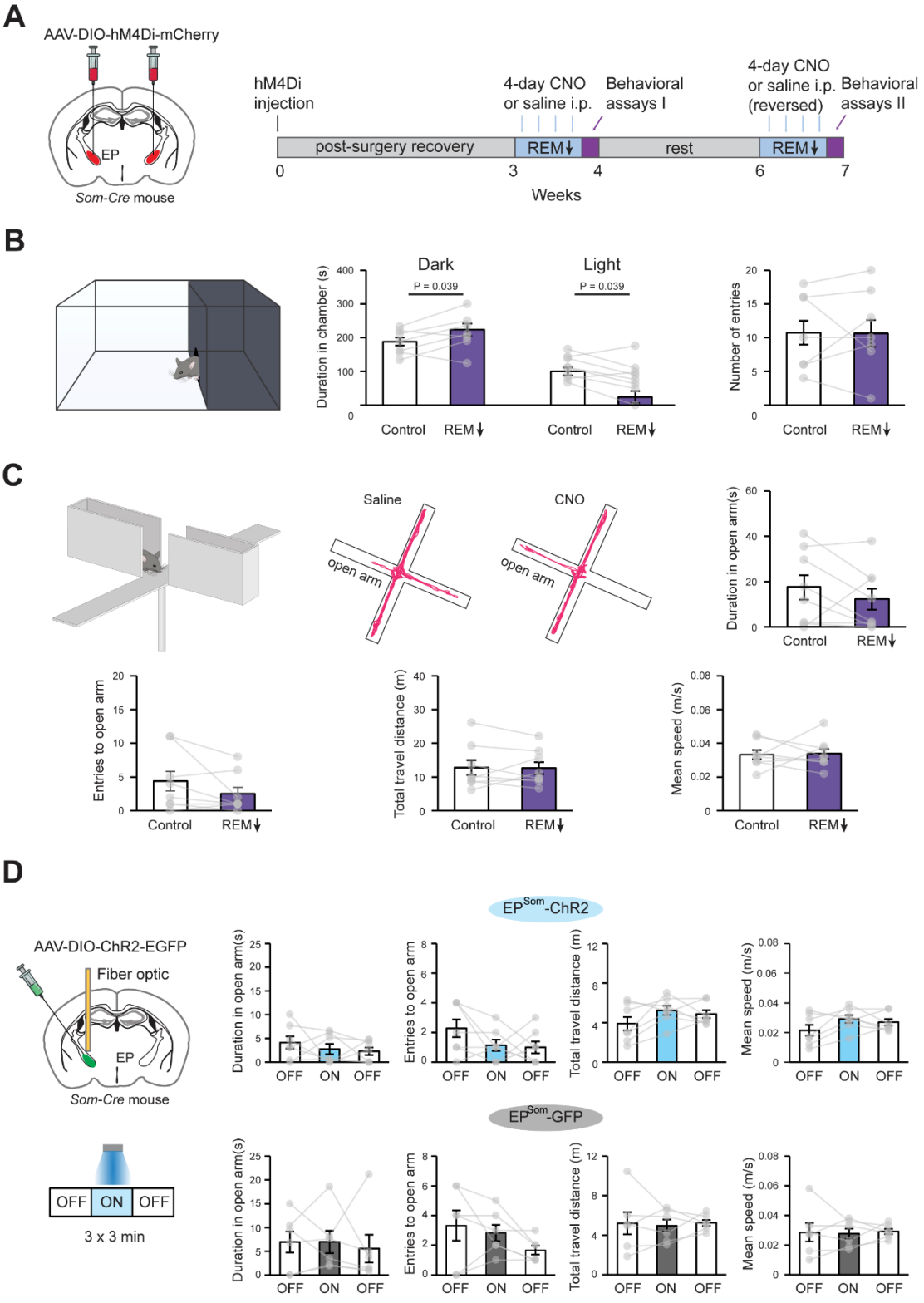
A
AAV-DIO-hM4Di-mCherry
EP
Som-Cre mouse
hM4Di injection
4-day CNO or saline i.p.
Behavioral assays I
4-day CNO or saline i.p. (reversed)
Behavioral assays II
post-surgery recovery
REM↓
rest
REM↓
0
3
4
6
7
Weeks
B
Dark
Light
P = 0.039
P = 0.039
Duration in chamber (s)
Number of entries
Control
REM↓
C
Saline
CNO
open arm
Duration in open arm(s)
Entries to open arm
Total travel distance (m)
Mean speed (m/s)
D
EP^Som-ChR2
EP^Som-GFP
AAV-DIO-ChR2-EGFP
Fiber optic
EP
Som-Cre mouse
OFF
ON
OFF
3 x 3 min

Figure S14 Effects of 4-day inhibition of EP neuronal activity on anxiety-like behaviors. Related to Figure 6.

(A) Schematic illustration of experimental setup. Three weeks following transduction of EP neurons in *Som-Cre* mice with *AAV-DIO-hM4Di-mCherry*, one systemic injection of CNO (1mg/kg *i.p.*), or saline, each day for 4 days and behavioral assays were carried out 16 hours after the last saline or CNO administration. After two weeks of rest, saline, or CNO (1mg/kg *i.p.*), was then injected *i.p.* in a counterbalanced manner, followed by a repeat of the behavioral tests. (B) Light/Dark box assay. Following 4-day inhibition of EP^{Som} neurons, mice spent significantly more time in the dark region, compared to the light region (n = 7). The motor activity, as assessed by the number of entries was unchanged. (C) Elevated plus maze following the manipulation of EP^{Som} neurons for 4 days. No significant changes were observed. (D) Acute activation of EP^{Som} neurons using optogenetic approach did not change behaviors in the elevated plus maze test. All data are means ± SEMs; P values are given when <0.05.